Plant Physiology®

Research Article

mRNA surveillance complex PELOTA–HBS1 regulates phosphoinositide-dependent protein kinase1 and plant growth

Wei Kong,[1,†] Shutang Tan,[2,3,†] Qing Zhao,[1] De-Li Lin,[4] Zhi-Hong Xu,[1] Jiří Friml [ID] [3] and Hong-Wei Xue [ID] [4,*,‡]

1 National Key Laboratory of Plant Molecular Genetics, CAS Centre for Excellence in Molecular Plant Sciences, Chinese Academy of Sciences, Shanghai, 200032, China
2 School of Life Sciences, Division of Life Sciences and Medicine, and Division of Molecular & Cell Biophysics, Hefei National Science Centre for Physical Sciences at the Microscale, University of Science and Technology of China, Hefei, 230027, China
3 Institute of Science and Technology Austria (IST Austria), Am Campus 1, Klosterneuburg, 3400, Austria
4 Joint Centre for Single Cell Biology, School of Agriculture and Biology, Shanghai Jiao Tong University, Shanghai, 200240, China

*Author for communication: hwxue@sjtu.edu.cn
†These authors contributed equally to this work (W.K., S.T.).
‡Senior author.

Abstract

The quality control system for messenger RNA (mRNA) is fundamental for cellular activities in eukaryotes. To elucidate the molecular mechanism of 3′-phosphoinositide-dependent protein kinase1 (PDK1), a master regulator that is essential throughout eukaryotic growth and development, we employed a forward genetic approach to screen for suppressors of the loss-of-function T-DNA insertion double mutant *pdk1.1 pdk1.2* in *Arabidopsis thaliana*. Notably, the severe growth attenuation of *pdk1.1 pdk1.2* was rescued by *sop21* (suppressor of *pdk1.1 pdk1.2*), which harbors a loss-of-function mutation in *PELOTA1* (*PEL1*). PEL1 is a homolog of mammalian PELOTA and yeast (*Saccharomyces cerevisiae*) DOM34p, which each form a heterodimeric complex with the GTPase HBS1 (HSP70 SUBFAMILY B SUPPRESSOR1, also called SUPERKILLER PROTEIN7, SKI7), a protein that is responsible for ribosomal rescue and thereby assures the quality and fidelity of mRNA molecules during translation. Genetic analysis further revealed that a dysfunctional PEL1–HBS1 complex failed to degrade the T-DNA-disrupted *PDK1* transcripts, which were truncated but functional, and thus rescued the growth and developmental defects of *pdk1.1 pdk1.2*. Our studies demonstrated the functionality of a homologous PELOTA–HBS1 complex and identified its essential regulatory role in plants, providing insights into the mechanism of mRNA quality control.

Open Access

Introduction

Living organisms need to monitor both the quantity and the quality of biomolecules, such as nucleic acids and proteins, to accomplish various life activities. Protein quality control is ensured by many levels of regulation for which messenger RNA (mRNA) quality is essential for biosynthesis of the correct corresponding protein: transcriptional, post-transcriptional, translational, and post-translational. The quality and fidelity of mRNAs are monitored by cells autonomously, and aberrant mRNAs need to be recognized by intrinsic molecular machineries to release stalled ribosomes and get degraded themselves (Tsuboi et al., 2012). According to current understandings, there are at least three different mRNA surveillance mechanisms: nonsense-mediated decay (NMD), no-stop decay (NSD), and no-go decay (NGD). NMD and NSD target mRNAs with premature stop codons (terminated too soon) and lacking stop codons (failing to terminate), respectively. NGD targets mRNAs stalled during translational elongation, e.g. those mRNAs with secondary structures or modifications. In mammals and yeasts, the PELOTA–HBS1 (Dom34p-HBS1p in yeasts) complex plays an essential role in regulating ribosomal rescue by recognizing the stalled ribosomes to initiate their recycling; this complex has been reported as important for all NMD, NSD, and NGD mechanisms (Shoemaker et al., 2010; Hilal et al., 2016). However, little was known about the mRNA quality control in plants so far.

3′-Phosphoinositide-dependent protein kinase1 (PDK1) is conserved in eukaryotes and plays important roles in regulating growth and development in various organisms (Pearce et al., 2010). As a key member of the cAMP-dependent protein kinase A/protein kinase G/protein kinase C (AGC) kinase family (Alessi, 2001), PDK1 is important for the activation of many AGC kinases and other substrates/regulators. Studies have revealed that PDK1 plays crucial roles in the signaling pathways activated by growth factors and hormones, sustains and regulates the balance among cell growth, division, and apoptosis in mammals (Alessi, 2001; Storz and Toker, 2002; Mora et al., 2004), and thus is critical for growth and development. However, loss-of-function mutation of PDK1 is lethal in various species, such as yeasts (Saccharomyces cerevisiae; Casamayor et al., 1999; Inagaki et al., 1999), fruit flies (Drosophila melanogaster; Rintelen et al., 2001), and mice (Mus musculus; Lawlor et al., 2002), which makes it challenging to study the downstream regulation, and the functional mechanism of PDK1 is still not completely understood.

Differently from mammals, loss-of-function or knockdown pdk1 mutant plants are viable, despite exhibiting severe developmental defects, as observed in rice (Matsui et al., 2010), Arabidopsis (Camehl et al., 2011; Tan et al., 2020; Xiao and Offringa, 2020), and moss (Dittrich and Devarenne, 2012). Therefore, plant models provide a more attractive approach to further identify the genetic interactors of PDK1. There are two PDK1 paralogs in Arabidopsis, PDK1.1 and PDK1.2 (also called PDK1 and PDK2), which have redundant functions (Dittrich and Devarenne, 2012; Tan et al., 2020; Xiao and Offringa, 2020). PDK1 binds to phospholipids, which regulates its activity as well as its subcellular localization (Deak et al., 1999; Anthony et al., 2004; Tan et al., 2020). As a master regulator of the AGC family, PDK1 was proposed to participate in various growth and developmental processes by phosphorylating distinct kinase substrates (Zegzouti et al., 2006b; Tan et al., 2020, 2021; Xiao and Offringa, 2020). For example, PDK1.1 regulates root hair development through phosphorylating OXIDATIVE SIGNAL INDUCIBLE1 (OXI1)/AGC2-1 kinase (Anthony et al., 2004; Rentel et al., 2004). PINOID (PID), an essential regulator of PIN-FORMED (PIN) auxin efflux carriers, was phosphorylated by PDK1 and thus activated in vitro (Friml et al., 2004; Zegzouti et al., 2006a). Recently, the characterization of the knockout pdk1.1 pdk1.2 double mutants uncovered the important role of plant PDK1. Both PDK1.1 and PDK1.2 are expressed in vascular tissues and show a predominant localization at the basal side of cell plasma membrane (PM) as well as at cytoplasm in root stele (Tan et al., 2020; Xiao and Offringa, 2020). Notably, the pdk1.1 pdk1.2 double mutants has pleotropic defects throughout growth and development, revealing an essential function of PDK1 in many life activities (Tan et al., 2020; Xiao and Offringa, 2020). Importantly, the basal localization of PDK1 dominates the role of AGC kinase substrates with the same subcellular distribution, including D6 Protein Kinase (D6PK)/D6 Protein Kinase Likes (D6PKLs; Zourelidou et al., 2009) and PROTEIN KINASE-ASSOCIATED WITH BRX (PAX; Marhava et al., 2018), to jointly participate in the regulation of polar auxin transport (Tan et al., 2020, 2021; Xiao and Offringa, 2020).

To further identify regulators involved in the PDK1 pathway, a forward genetic approach was employed. Using an ethyl methanesulfonate (EMS) population of Arabidopsis pdk1.1 pdk1.2 double mutant that displayed severe growth defects, a suppressor screening was performed. In this study, characterization of an identified mutant, sop21 (suppressor of pdk1.1 pdk1.2), reveals that deficiency of the translational mRNA surveillance complex PELOTA–HBS1 rescues the defective phenotype of pdk1.1 pdk1.2. Our studies demonstrate the functionality of a homologous PELOTA–HBS1 complex in plants and provide informative clues on the control of mRNA surveillance and thus protein homeostasis.

Results

Deficiency of *PEL1* suppresses the defective growth of Arabidopsis *pdk1.1 pdk1.2*

Two paralogous PDK1 genes in Arabidopsis thaliana, PDK1.1 (AT5G04510) and PDK1.2 (AT3G10540; Camehl et al., 2011; Dittrich and Devarenne, 2012; Tan et al., 2020), exhibit overlapping and widespread expression patterns in various tissues, as revealed by quantitative polymerase chain reaction (PCR) and GUS staining analyses (Supplemental Figure S1).

Notably, both *PDK1.1* and *PDK1.2* were detected to be expressed in seedlings, roots, rosette leaves, cauline leaves, stems, flowers, and siliques, with strong expression in vascular tissues (Supplemental Figure S1), similar as previously reported (Tan et al., 2020). The *pdk1* single loss-of-function mutants, *pdk1.1-2* and *pdk1.2-4* (hereafter as *pdk1.1* and *pdk1.2*, respectively), displayed no obvious growth phenotype (Tan et al., 2020), whereas the double mutant *pdk1.1 pdk1.2* exhibits a range of developmental defects (Figure 1; Supplemental Figure S2), including suppressed growth (smaller leaves and shorter siliques), reduced axillary shoots, suppressed primary root elongation and lateral root initiation, substantially decreased fertility, and abnormal floral development (Tan et al., 2020). This is consistent with the crucial roles of PDK1 in other organisms and confirms the essential role of *PDK1* in regulating plant growth and development. Several aspects of those developmental defects can be explained by known AGC kinases, such as D6PK (Tan et al., 2020), PAX (Xiao and Offringa, 2020), and AGC1.5/7 (Zhang et al., 2009; Xiao and Offringa, 2020). However, whether there are additional components in the PDK1 pathway, other than AGC kinases, remains unclear.

To elucidate the underlying mechanism of PDK1 function, a forward genetic screen was performed. Seeds of *pdk1.1 pdk1.2* were used to generate a mutant population by EMS mutagenesis, and suppressors of *pdk1.1 pdk1.2* (*sop*, suppressor of *pdk1.1 pdk1.2*) were screened based on rescued growth (Page and Grossniklaus, 2002). More than 10 suppressors were obtained from a M_2 population of approximately 80,000 plants, and a recessive mutant, *sop21*, that showed obviously rescued growth of *pdk1.1 pdk1.2* (Figure 1; Supplemental Figure S2), was characterized first. Compared to the significantly suppressed growth of *pdk1.1 pdk1.2* adult plants, the rosette size of *pdk1.1 pdk1.2 sop21* is comparable to that of wild-type (WT; Figure 1A; Supplemental Figure S2D). Similar degree of rescue was also observed for the fertility, silique length, inflorescence morphology, and floral development (Figure 1, B and C; Supplemental Figure S2, E and F). Notably, the lateral root numbers were only partially rescued to ∼50% of WT, though with a complete rescue of primary root growth (Figure 1, D–F).

To identify the causative mutation in *sop21*, 102 progenies (referred as BC_1F_2) showing rescue phenotypes were selected from a segregating pool of backcross F_2 individuals (102 rescued phenotype: 296 *pdk1.1 pdk1.2* phenotype, for 1:3 ratio [$\chi^2 = 0.084$, $P > 0.75$; Chi-square test], which indicated a causal single recessive mutation) and used for DNA extraction and subsequent deep sequencing (Allen et al., 2013). Systemic analysis revealed that *sop21* carried a mutation in *PEL1* (*AT4G27650*; Csorba et al., 2018), which led to an early stop at amino acid residue 27 (tryptophan to terminator, W27*), resulting in the translationally premature termination (Supplemental Figure S2A). Reverse transcription quantitative real-time PCR (RT-qPCR) and GUS staining analyses revealed that the *PEL1* gene was expressed in seedlings, roots, rosette leaves, cauline leaves, stems, flowers, and

siliques, with elevated expression in vascular tissues (Supplemental Figure S3), which is similar to the expression of *PDK1s*. Cross of a null T-DNA insertional allele *pel1* (*SALK_124403*, also named *lesion mimic leaf1-1*, *lml1-1*; Qin et al., 2018; Supplemental Figure S2, B and C) with *pdk1.1 pdk1.2* also suppressed the growth defects of *pdk1.1 pdk1.2* at various aspects (Figure 1), verifying that the suppression of *pdk1.1 pdk1.2p* phenotype in *sop21* was a result of *PEL1* deficiency. Though *pel1* mutant was previously shown to exhibit a reduced growth rate (Qin et al., 2018), both *sop21* and *pel1* mutants grew normally in our hands, perhaps due to different growth conditions. In addition, the expression of *PEL1–FLAG* driven by a *CaMV35S* promoter in *sop21* restored the *pdk1.1 pdk1.2* phenotype (Supplemental Figure S4, A and B), confirming that *PEL1* deficiency suppressed the growth defects of *pdk1.1 pdk1.2*. The overexpression of *PEL1–FLAG* driven by *CaMV35S* in WT background did not exhibit any obvious phenotype (Supplemental Figure S4, C and D).

Next, we constructed *35S::PEL1–GREEN FLUORESCENT PROTEIN (GFP)* and *35S::mCherry–PEL1* transgenic plants to study the subcellular localization of PEL1. We observed the presence of PEL1–GFP and mCherry–PEL1 in the cytoplasm and nucleus (Figure 2A). The subcellular localization of PEL1 partially overlapped with that of PDK1.1, which also showed residence in cytoplasm, but PEL1–GFP did not share the PM localization with PDK1.1 (Figure 2A). Further analysis using tobacco leaves revealed that both mCherry–PEL1 (Figure 2B) and mCherry–PDK1.1 (Figure 2C) did not distribute equally in cytoplasm, and indeed they exhibited a similar feature in that both proteins localized to certain compartments associated with endoplasmic reticulum (ER).

Presence of the mRNA surveillance complex PELOTA–HBS1 in Arabidopsis

Most of our knowledge about the PELOTA–HBS1 complex function comes from the studies in animals and yeast. Translation of aberrant mRNAs leads to stalling of translational machinery, and arrested ribosomes are specifically recognized by the PELOTA–HBS1 complex to initiate their recycling (Shoemaker et al., 2010; Pisareva et al., 2011; Tsuboi et al., 2012; Saito et al., 2013). Mammalian and yeast PELOTA/DOM34p interact with the HBS1 GTPase, a translation elongation factor EF1A/initiation factor IF2γ family protein, to form a heterodimer and bind to stalled ribosomes, ultimately leading to ribosome rescue. Furthermore, HBS1 is involved in post-transcriptional gene silencing (Csorba et al., 2018; Lange et al., 2019). Homology analysis in Arabidopsis genome by using yeast and human HBS1 identified two candidate HBS1 homologs, AT5G10630 and AT1G18070. Sequence alignment analysis showed that only AT5G10630 had the conserved HBS1_C domain, indicating that AT5G10630 (designated as AtHBS1, HBS1) is the HBS1 homolog in Arabidopsis (Supplemental Figure S5). As reported previously, AT1G18070 is a close homolog of eukaryotic release factor 3, which terminates translation and releases
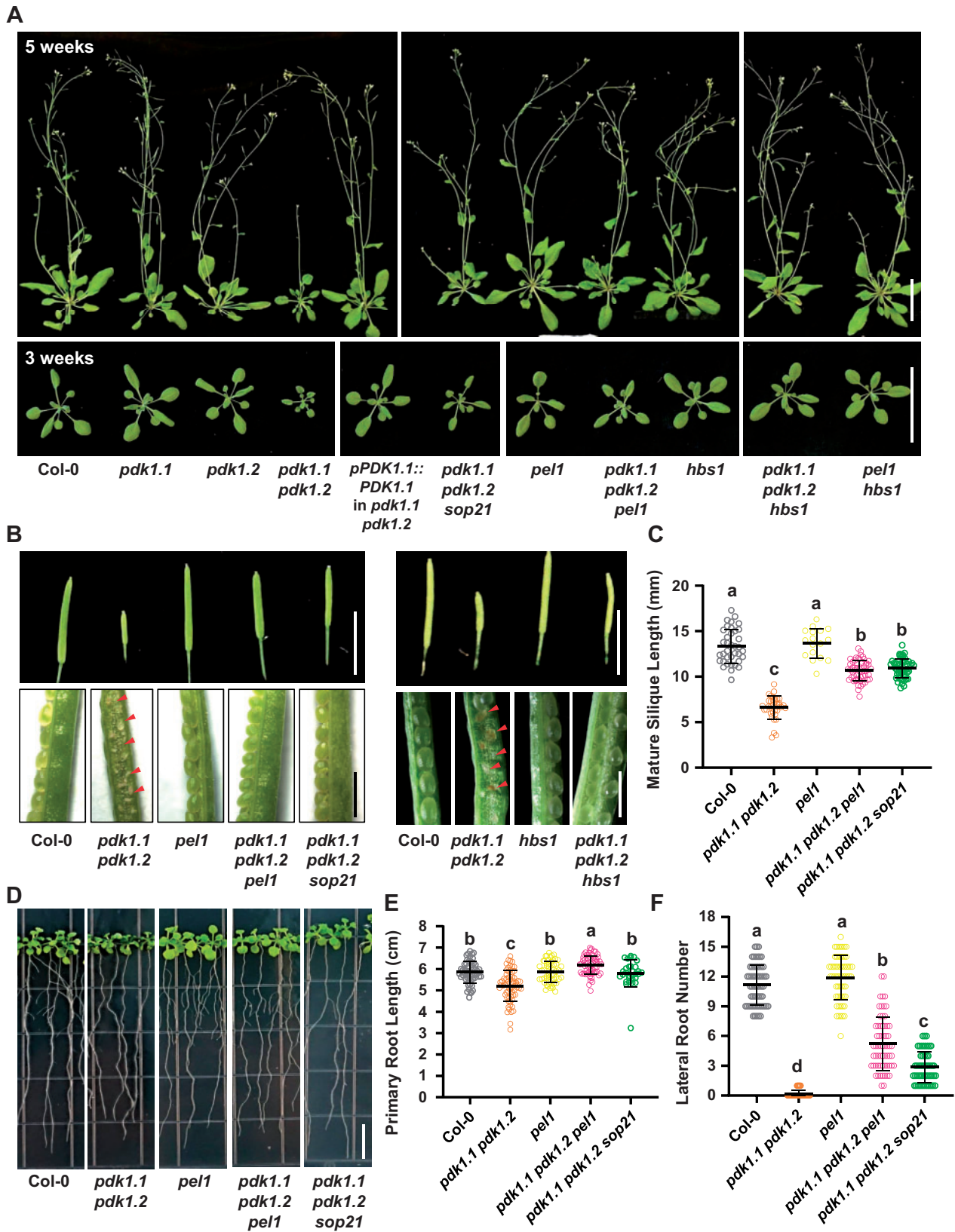
Figure 1 The *sop21* mutation or deficiency of *PEL1* or *HBS1* restores the growth defects of *Arabidopsis pdk1.1 pdk1.2* double mutant. A, The *sop21* mutation or loss of function of *PEL1* or *HBS1* suppresses the growth defect of *pdk1.1 pdk1.2*, including the reduced growth and delayed bolting. 3- or 5-week-old Col-0, *pdk1.1 pdk1.2*, *pdk1.1 pdk1.2 pel1*, *pdk1.1 pdk1.2 sop21* (*pdk1.1 pdk1.2 pel1^{W27*}*), *pdk1.1 pdk1.2 hbs1* and various mutant plants are shown. Scale bars, 5 cm. B, Siliques and setting rate of Col-0 and various mutants. Scale bars, 2 cm (upper) or 1 mm (lower). Defective/abnormal seeds of *pdk1.1 pdk1.2* are highlighted with red arrowheads. C, Quantification of the silique lengths of Col-0 and various

ribosomes (Brunkard and Baker, 2018). Considering that HBS1 functions in the same pathway as PEL1 in Arabidopsis (Csorba et al., 2018), it was then chosen for further investigations. Indeed, analyses of yeast two-hybrid (Figure 3A), bimolecular fluorescence complementation (BiFC; Figure 3B) and GST pull-down assays (Figure 3C) revealed the PEL1–HBS1 interactions both in vivo and in vitro, confirming the presence of a homologous PELOTA–HBS1 complex in plants. In addition, a recent study in plants characterizing the roles of PELOTA and HBS1 in nonstop mRNA decay (Csorba et al., 2018) further supports the presence of a functional PELOTA–HBS1 complex in Arabidopsis. However, whether the PELOTA–HBS1 complex participates in other types of mRNA surveillance mechanisms requires further investigations.

Similarly to PEL1 and PDK1s, the HBS1 gene was ubiquitously expressed (Supplemental Figure S6A) and a knockdown mutant of HBS1, hbs1 (Supplemental Figure S6, B–D) also suppressed the pdk1.1 pdk1.2 phenotypes (Figure 1, A and B), indicating that deficiency of the translational mRNA surveillance complex PELOTA–HBS1 led to the suppression of pdk1.1 pdk1.2 phenotypes. These observations physically and functionally support the existence of PELOTA–HBS1 complex.

PELOTA–HBS complex regulates the degradation of aberrant *PDK1* transcripts

The pdk1.1-2 and pdk1.2-4 alleles we used contain T-DNA insertions close to their 3′-ends. It has been speculated by Xiao and Offringa (2020) that such alleles are likely to lead to the production of a functional truncated protein. Therefore, in the same publication, this was proposed to explain the lack of strong phenotypes for double mutant combinations pdk1.1-2 pdk1.2-2 and pdk1.1-2 pdk1.2-3 observed in previous studies (Camehl et al., 2011; Scholz et al., 2019). However, it is unlikely that a partially functional truncated protein could explain the previous failure to observe the obvious defects in these alleles, since recent studies by Tan et al. (2020) and Xiao and Offringa (2020) both reported highly similar phenotypes for different allele combinations. Further comparisons confirmed that the pdk1.1 pdk1.2 (pdk1.1-2 pdk1.2-4) alleles used here in our study, as well as double mutants generated with pdk1.1-2 and other pdk1.2 T-DNA alleles, recapitulated the phenotype of double mutant combinations with the CRISPR alleles pdk1.1-13 or pdk1.1-14 reported by Xiao and Offringa (2020;

Supplemental Figure S7, A and B). Therefore, we speculate that previous failures to observe strong growth and development defects in pdk1.1-2 pdk1.2-2 or pdk1.1-2 pdk1.2-3 double mutant lines (Camehl et al., 2011; Scholz et al., 2019) are most likely due to a failure to achieve true double homozygous plants.

Interestingly, we also noted that the rosette size of pdk1.1 pdk1.2 plants is larger than other double mutant combinations, suggesting the remaining function of PDK1s (Supplemental Figure S8). RT-qPCR analysis revealed that there was no detectable expression of either PDK1.1 or PDK1.2 in pdk1.1 pdk1.2 backgrounds, with the primers amplifying regions across T-DNA insertions (Figure 4, A and B), ruling out the possibility of existing full-length PDK1.1 or PDK1.2 transcripts. Nonetheless, when primers amplified the fragments before T-DNA insertions, we detected increased levels of truncated transcripts of PDK1.1 and PDK1.2 (to ∼50% or 90% of Col-0, respectively) in pdk1.1 pdk1.2 sop21, pdk1.1 pdk1.2 pel1, and pdk1.1 pdk1.2 hbs1, compared to those in pdk1.1 pdk1.2 (10% and 25% of Col-0 for PDK1.1 and PDK1.2, respectively; Figure 4, C and D). The decrease of PDK1.1 and PDK1.2 transcripts was further confirmed by semi-quantitative PCR analysis (Supplemental Figure S8A). The PELOTA–HBS1 complex is responsible for the release of arrested ribosomes during the translation of aberrant mRNAs, so called "mRNA surveillance", and these mRNAs are degraded (Csorba et al., 2018). T-DNA insertions at the 3′-ends of PDK1.1 and PDK1.2 coding regions might lead to aberrant PDK1.1 and PDK1.2 transcripts fused with a partial T-DNA fragment, and these mRNAs could be degraded by the mRNA surveillance mechanisms. Therefore, our observation that only 10% and 25% of PDK1.1 and PDK1.2 5′-fragments were detected in pdk1.1 pdk1.2 confirms the instability of these transcripts in planta. Notably, there was an increase of their expressions in pdk1.1 pdk1.2 sop21, pdk1.1 pdk1.2 pel1, or pdk1.1 pdk1.2 hbs1 plants. The above observations suggested that the decay of aberrant PDK1.1 and PDK1.2 transcripts is mediated by the PEL1–HBS1-mediated mRNA surveillance mechanism. This led us to test whether the increased levels of truncated PDK1.1 or PDK1.2 could explain the rescue of pdk1.1 pdk1.2.

By transforming an mCherry-fused PDK1.1N (1–399 aa; Tan et al., 2020) driven by pPDK1.1 promoter into pdk1.1 pdk1.2, a partial rescue was observed (Figure 4E). In addition, the overexpression of Venus-PDK1.1N or Venus-PDK1.2N (encoding 1–394 aa) driven by a CaMV35S promoter

mutants. Data are presented as means ± SD ($n > 30$). $n = 37, 36, 17, 54$, and 51 siliques for Col-0, pdk1.1 pdk1.2, pel1, pdk1.1 pdk1.2 pel1, and pdk1.1 pdk1.2 sop21, respectively. Different letters represent significant differences, $P < 0.05$. Corrected P-values were calculated by one-way ANOVA with a Tukey's multiple comparison test. D, Root elongation and lateral root formation of Col-0 and various mutants. Two-week-old seedlings were observed. Scale bar, 1 cm. Representative images are shown. E, Lengths of primary roots of 2-week-old Col-0 and various mutants were calculated. Data are presented as means ± SD ($n > 30$). n = 56, 65, 52, 62, and 30 plants for Col-0, pdk1.1 pdk1.2, pel1, pdk1.1 pdk1.2 pel1, and pdk1.1 pdk1.2 sop21, respectively. Different letters represent significant differences, $P < 0.05$. Corrected P-values were calculated by one-way ANOVA with a Tukey's multiple comparison test. F, Numbers of emerged lateral roots of 2-week-old Col-0 and various mutants were counted. Data are presented as means ± SD ($n > 30$). $n = 61, 65, 63, 63$, and 52 plants for Col-0, pdk1.1 pdk1.2, pel1, pdk1.1 pdk1.2 pel1, and pdk1.1 pdk1.2 sop21, respectively. Different letters represent significant differences, $P < 0.01$. Corrected P-values were calculated by one-way ANOVA with a Tukey's multiple comparison test.
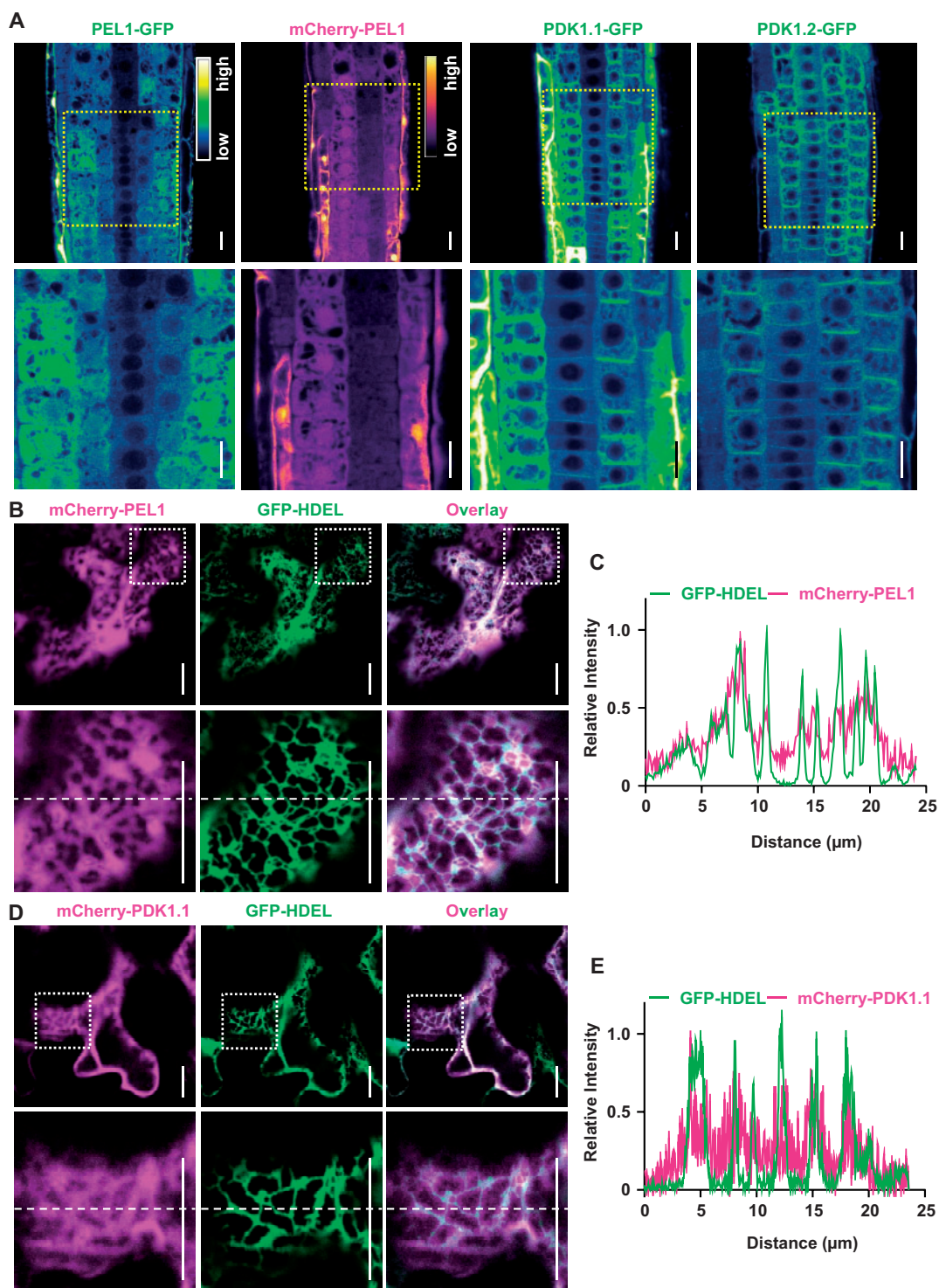
Figure 2 Subcellular localizations of PEL1 and PDK1.1. A, Stable *transgenic* lines revealed that PEL1 localized to the cytoplasm and nucleus, and that PDK1.1-GFP and PDK1.2-GFP resided at PM and cytoplasm. Five-day-old *35S::PEL1-GFP*, *35S::mCherry-PEL1*, *35S::PDK1.1-GFP*, and *35S::PDK1.2-GFP* T_2 seedlings were observed by CLSM. The "Green Fire Blue" LUT was used for GFP, and "mpl-inferno" LUT was used for mCherry visualizations, based on fluorescence intensity (as indicated by the color scale) by Fiji. Lower panels are enlarged view of the squared region of the upper panels. Scale bars, 20 μm. At least three independent lines were obtained for each genotype, and similar localizations were observed. Representative images are shown. n = 7, 8, 10, 12 individual plants for *35S::PEL1-GFP*, *35S::mCherry-PEL1*, *35S::PDK1.1-GFP* and *35S::PDK1.2-GFP*, respectively. B–E, *Fluorescence* observations showed that both PEL1 and PDK1.1 localized to certain cytoplasm compartments associated with the ER. Fusion proteins mCherry-PEL1 (B and C) and mCherry-PDK1.1 (D and E) were transiently expressed with ER-specific GFP-HDEL proteins in tobacco leaves. Samples were observed 48 h after infiltration. Scale bars, 20 μm. Lower parts are enlarged view of the squared region of the upper parts. The position for quantification (right) was indicated with dashed lines across the images. Each pair of transformations was performed with five leaves and repeated twice. n = 10 and 11 samples for mCherry-PEL1+GFP-HDEL and mCherry-PDK1.1+GFP-HDEL, respectively.
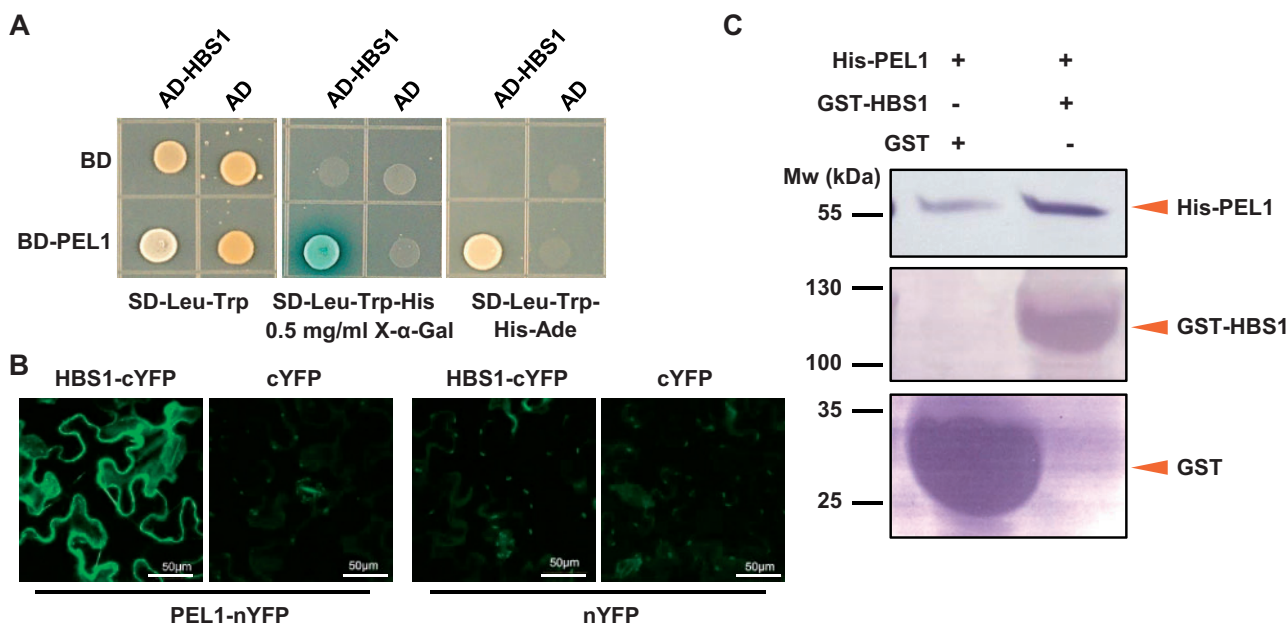
Figure 3 PEL1 forms a complex with HBS1. A, B, Yeast two-hybrid (A) and BiFC (B) analyses reveal the interactions of PEL1 with HBS1. PEL1 and HBS1 were fused to GAL4 DNA-binding domain (BD) or activation domain (AD), respectively. Protein interaction was examined on synthetic dropout (-Leu/-Trp/-His) medium supplemented with 0.5 mg·mL^{-1} X-α-Gal, or synthetic dropout (-Leu/-Trp/-His-Ade) medium. For BiFC analysis, PEL1–nYFP or HBS1–cYFP fusion proteins were transiently expressed in *N. benthamiana* leaves through infiltration and observed. Scale bars, 50 μm. C, GST pull-down analysis reveals the interactions of PEL1 with HBS1. GST and GST-HBS1 fusion protein were used as baits, and 6×His-PEL1 fusion protein was used as prey. Pulled-down fractions were analyzed by Western blot using anti-His and anti-GST antibodies. Red arrowheads indicate corresponding bands.

completely rescued the phenotype of *pdk1.1 pdk1.2* (Supplemental Figure S8B). Therefore, we conclude that the *pel1* and *hbs1* mutations might rescue the phenotype of *pdk1.1 pdk1.2* via disrupting the function of PELOTA–HBS1 mRNA surveillance complex, and thus upregulating the amount of N-terminal truncated proteins of PDK1.1 and PDK1.2, which preserve functional kinase activity (Xiao and Offringa, 2020). Further genetic analysis on these double mutants by Xiao and Offringa (2020) and *pel1* might help to confirm whether these effects are allele-specific.

PDK1 regulates development and stress responses through coordinating multiple metabolic pathways

The PELOTA–HBS1 complex regulates the mRNA quality control by rescuing stalled ribosomes during protein biosynthesis (Csorba et al., 2018). PDK1 is also an essential regulator of protein translation, via modulating the activity of ribosome RPS6 proteins through S6K AGC kinase (Mahfouz et al., 2006; Pearce et al., 2010; Kim et al., 2014). We therefore performed a proteomic analysis to study their functions at the proteome level. First, subcellular localization both of stable transgenic seedlings and of seedlings transiently expressing YFP- or GFP-fused proteins in Arabidopsis leaf protoplasts (from adult Col-0 plants) and tobacco leaves clearly showed that PDK1, PEL1, and HBS1 proteins located at the PM and cytoplasm (Figure 2B; Supplemental Figure S9). Intriguingly, PDK1 and PEL1 exhibited compartmentalized localization at the cytoplasm, associated with ER (Figure 2B). In addition, PEL1–YFP exhibits nuclear

distribution, which was undetectable for PDK1s and HBS1 (Figure 2A; Supplemental Figure S9, A and B). The different subcellular localizations of PEL1 and HBS1 proteins suggest they might have differential functions beyond their roles in mRNA surveillance.

A tandem mass tag (TMT)-based comparative proteomics analysis was then performed using shoots and roots of 2-week-old Col-0, *pdk1.1 pdk1.2* and *pdk1.1 pdk1.2 pel1* seedlings, and 6,995 and 8,137 proteins were quantified in shoots (Supplemental Table S1) and roots (Supplemental Table S2). We studied shoots and roots separately because they might have different proteomes. Of the identified proteins, 71 (out of 111 changed proteins in total) and 56 (out of 113) proteins in shoots (Supplemental Tables S3 and S4) or roots (Supplemental Tables S5 and S6), respectively (Figure 5, A and B), were significantly changed in *pdk1.1 pdk1.2*, while rescued in *pdk1.1 pdk1.2 pel1* to similar levels as in WT. These changed proteins were designated as restored commonly expressed (RCE) proteins and were speculated as being responsible for the defective growth of *pdk1.1 pdk1.2*.

KEGG analysis of RCE proteins revealed that *pdk1.1 pdk1.2* exhibited enriched metabolic pathways, including for lipids, carbohydrates, phenylpropanoid, and amino acids, as well as enrichment of proteins involved in multiple developmental processes and environmental adaptation (Table 1; Supplemental Tables S3 and S5), which was consistent with its general growth defects. A nitrogen-regulated glutamine amidotransferase GAT 1_2.1 that represses shoot branching (Zhu and Kranz, 2012) increased in *pdk1.1 pdk1.2*, which is
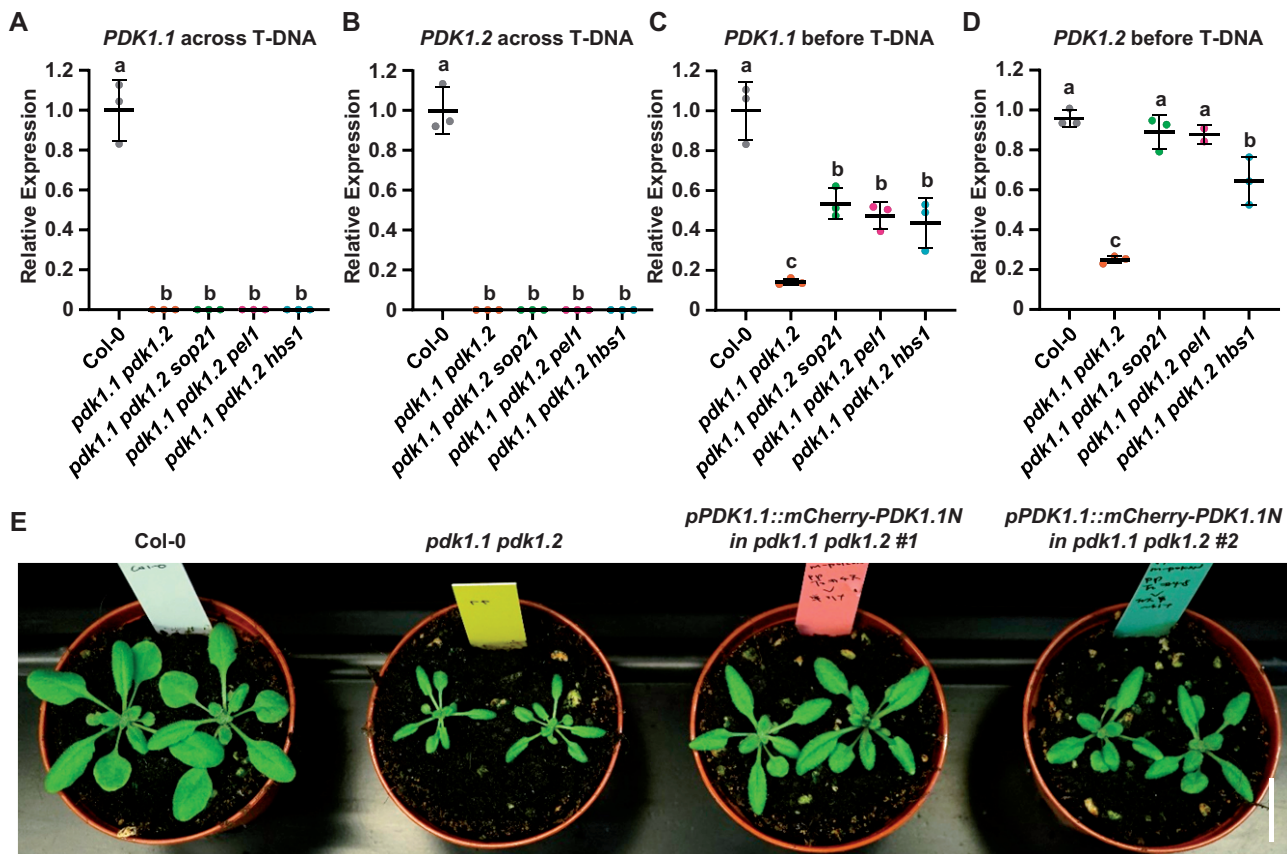
Figure 4 Increased expression of truncated *PDK1* transcripts in the *pdk1.1 pdk1.2 pel1* or *pdk1.1 pdk1.2 hbs1* background accounts for the rescued phenotypes. A and B, RT-qPCR analysis with primers amplifying regions across T-DNA insertions revealed that the integrity of *PDK1.1* and *PDK1.2* full-length CDS was disrupted by the T-DNA insertions in *pdk1.1 pdk1.2*, *pdk1.1 pdk1.2 sop21*, *pdk1.1 pdk1.2 pel1*, and *pdk1.1 pdk1.2 hbs1*. *ACTIN7* gene was amplified and used as an internal control. Experiments were biologically repeated three times and data are presented as means ± SD (n = 3). Different letters represent significant differences, $P < 0.05$. Corrected *P*-values were calculated by one-way ANOVA with a Tukey's multiple comparison test. C and D, RT-qPCR analysis with primers amplifying regions in front of T-DNA insertions revealed that N-terminal fragments of *PDK1.1* and *PDK1.2* transcripts (PDK1.1N and PDK1.2N) exhibited increased levels in *pdk1.1 pdk1.2 sop21*, *pdk1.1 pdk1.2 pel1*, and *pdk1.1 pdk1.2 hbs1*, respectively, compared to that in *pdk1.1 pdk1.2*. *ACTIN7* gene was used as an internal control. Experiments were biologically repeated three times and data are presented as means ± SD (n = 3). Different letters represent significant differences, $P < 0.05$. Corrected *P*-values were calculated by one-way ANOVA with a Tukey's multiple comparison test. E, Native promoter-driven expression of the PDK1 N-terminal fragment partially rescued the growth defects of *pdk1.1 pdk1.2*. A representative photo of 20-d-old Col-0, *pdk1.1 pdk1.2*, and *pPDK1.1::mCherry-PDK1.1N* (in *pdk1.1 pdk1.2*) plants grown in soil is shown. Scale bar, 2 cm.

consistent with the solitary stem phenotype of *pdk1.1 pdk1.2*. Furthermore, increased DUF642 family proteins DGR1 (DUF642 L-GALL-RESPONSIVE GENE1) and DGR2 (Gao et al., 2012), and several root hair-related proteins, including SEED AND ROOT HAIR PROTECTIVE PROTEIN, also called ROOT HAIR-SPECIFIC 13, RHS13 (Tanaka et al., 2017), PROLINE-RICH PROTEIN LIKE 1 (Boron et al., 2014), GH9C1 (one *GH9* gene containing a *CBM49*; Del Campillo et al., 2012), DEFORMED ROOT HAIRS 9, also called COBRA-LIKE 9, COBL9, MUTANT ROOT HAIR 4, MRH4, SHAVEN 2, SHV2 (Ringli et al., 2005), and OXI1 (Anthony et al., 2004; a known PDK1 substrate), may account for the altered root development.

A large number of pathogen-induced defense-related or systemic acquired resistance-related proteins (Thomma et al., 1998; Ferrari, 2003; Ferrari et al., 2007; Tronchet et al., 2010; Stotz et al., 2011; Jung et al., 2012; Breitenbach et al.,

2014; Chen et al., 2014; Weis et al., 2014) are accumulated in *pdk1.1 pdk1.2* (Table 1; Supplemental Tables S3 and S5). Meanwhile, some abiotic stress-related proteins, especially cold acclimation/responsive proteins (Horvath et al., 1993; Uemura et al., 2002; Guo et al., 2013; Dyson et al., 2016) significantly increased in *pdk1.1 pdk1.2* shoots. This is consistent with the previous studies showing that PDK1 positively regulates basal resistance to a blast fungus, *Magnaporthe oryzae*, and a bacterial pathogen, *Xanthomonas oryzae* pv. *Oryzae* (*Xoo*) in rice (Matsui et al., 2010), and that PDK1 is required for *Piriformospora indica*-induced growth promotion (Camehl et al., 2011). Together with the previous notion that AGC kinases are major substrates of PDK1 (Tan et al., 2020; Xiao and Offringa, 2020), we conclude that these changes at the proteome level might be indirectly regulated by PDK1 through certain downstream pathways.
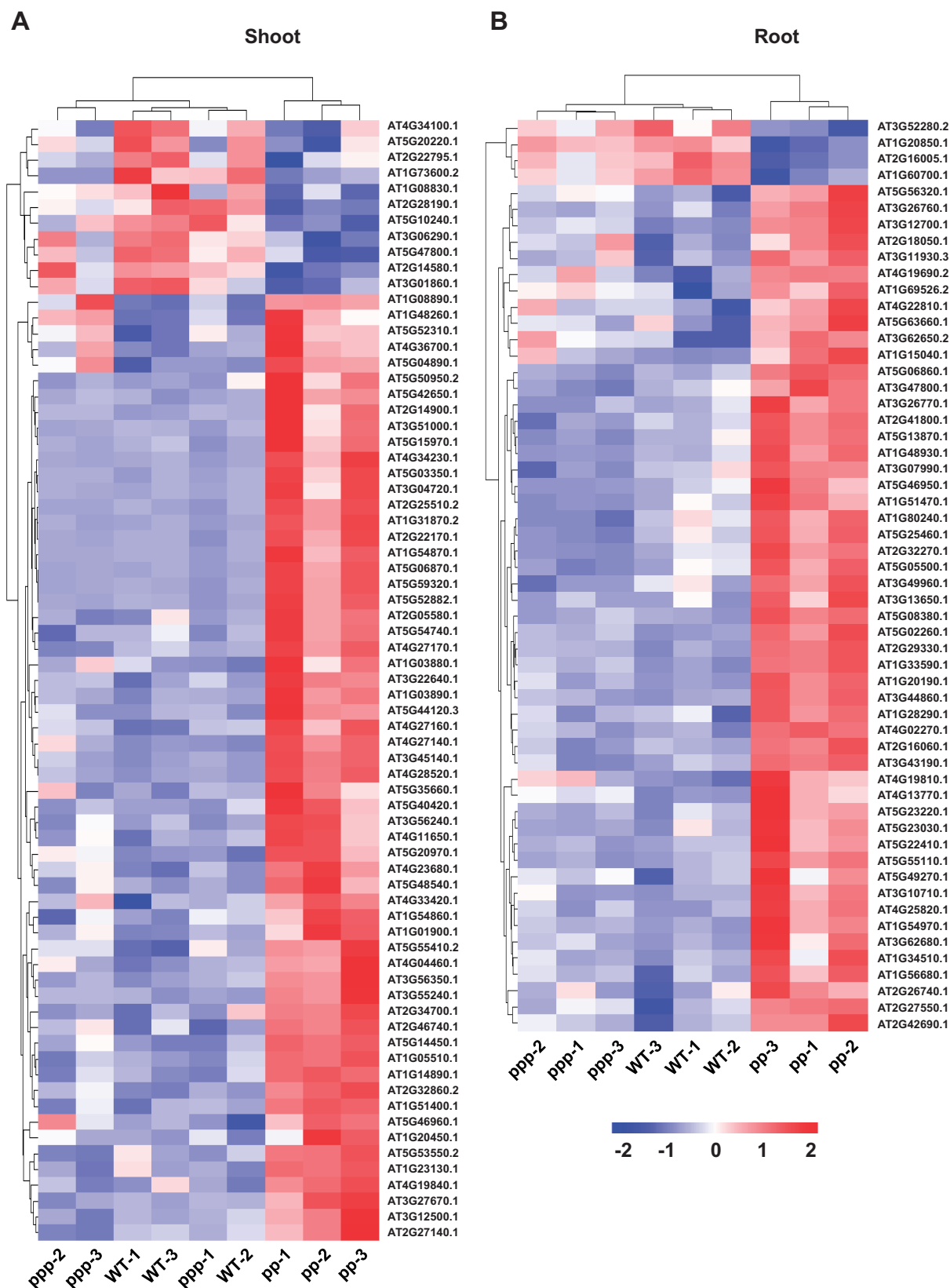
Figure 5 Comparative proteomics showing the functions of PDK1 and PEL1 in shaping the proteomes in Arabidopsis. Heat map displays the abundance of 71 RCEs in shoots (A, proteins listed in Supplemental Table S3) and 56 RCEs in roots (B, proteins listed in Supplemental Table S5) of WT Col-0, *pdk1.1 pdk1.2* and *pdk1.1 pdk1.2 pel1*. "pp" refers to *pdk1.1 pdk1.2* double mutant and "ppp" refers to *pdk1.1 pdk1.2 pel1* triple mutant. Three independent samples of WT (WT-1, -2, -3), *pdk1.1 pdk1.2* (pp-1, -2, -3), and *pdk1.1 pdk1.2 pel1* (ppp-1, -2, -3) were collected and analyzed. Heat maps were generated using log2-transformed TMT values. The color scale (from blue to red) indicates the protein levels. Relative level of RCE proteins was used to perform the hierarchical clustering analysis using the OECloud tools at https://cloud.oebiotech.cn.

Table 1 RCEs proteins identified by analyzing Col-0, *pdk1.1 pdk1.2*, and *pdk1.1 pdk1.2 pel1* mutants

Category	Definition	RCE proteins	*pdk1.1 pdk1.2*
Metabolisms	Lipid metabolism	Phospholipase A2 family protein PLA2α	De
		Lipoxygenase LOX2	In
		Lipid transport superfamily protein AT1G23130	In
		Lipid transfer protein LTP3	In
	Carbohydrate metabolism	Fumarase FUM2	In
		Galactose mutarotase-like protein AT3G47800	In
		Alpha-galactosidase AGAL1	In
		Xyloglucan endotransglucosylase/hydrolase XTH5	In
	Phenylpropanoid biosynthesis	Cinnamyl alcohol dehydrogenase	In
		Peroxidase superfamily proteins AT1G34510	In
		Peroxidase superfamily proteins PER4	In
		Peroxidase superfamily proteins AT3G49960	In
	Amino acid metabolism	Asparagine synthetase ASN3	De
		D-site 20S pre-rRNA nuclease AT5G41190	De
Development	Shoot branching	Nitrogen-regulated glutamine amidotransferase 1_2.1	In
	Root and rosette	DUF 642 family proteins DGR1	In
		DUF 642 family proteins DGR2	In
	Root hair	Root hair-specific 13 SRPP	In
		Proline-riched protein-like 1	In
		Glycosyl hydrolase 9C1 AtGH9C1	In
		Deformed root hair 9	In
	Embryo	Embryo defective 1923 (EMB1923)	De
		Resurrection1 RST1	In
		Yellow stripe like 3	In
	Chloroplast	Chloroplast division-related protein FAD6	De
		Chloroplast grana formation-related protein GDC1	De
Stress	Pathogen-induced defense / systemic acquired resistance	Pathogenesis-related 3	In
		Pathogenesis-related 4	In
		Cinnamyl alcohol dehydrogenase	In
		Yellow stripe like 3	In
		Flavin-binding monooxygenase family protein FMO	In
		Phospholipase A2 family protein PLA2α	De
		Legume lectin family protein LLP1	In
		Polygalacturonase inhibiting protein 2 AtPGIP2	In
		Polygalacturonase inhibiting protein 1 AtPGIP1	In
		CYP83A1	In
	Cold	Cold-responsive protein 6.6 COR6.6	In
		Cold-responsive protein 78 COR78	In
		Fumarase 2 FUM2	In
		Lipid transfer protein 3	In
Seed storage proteins	2S albumin	2S seed storage protein 1 AT2S126	In
		2S seed storage protein 3 AT2S3	In
		2S seed storage protein 4 AT2S4	In
		2S seed storage protein 5 AT2S5	In
	12S globulin	Vicilin-like seed storage protein AT4G36700	In
		Cruciferin A CRA1	In
		Cruciferin B CRB	In
		Cruciferin 2 CRU2	In
		Cruciferin 3 CRC	In
	Other nutrient reserve-related proteins	Lipid transfer protein	In
		Lipoxygenase protein LOX2	In
		Oleosin OLEO2	In
		Seed-specific protein AT2G05580	In

Proteins were functionally categorized by KEGG pathway analysis and information from previous studies. In, increased; De, decreased; SRPP, SEED AND ROOT HAIR PROTECTIVE PROTEIN.

Most RCE proteins showed increased levels (113 out of 127 proteins) in *pdk1.1 pdk1.2*, suggesting that PDK1 deficiency may lead to promoted protein biosynthesis. To test if PDK1 participates in the regulation of the PELOTA–HBS1 complex, we examined the protein levels of PEL1 and HBS1 in the TMT-based comparative proteomics datasets. Results showed that PEL1 and HBS1 exhibited unchanged protein

abundance in *pdk1.1 pdk1.2* (Supplemental Figure S10, A and B), which however can not exclude that PDK1 might regulate the PELOTA–HBS1 complex at the post-translational level.

PDK1 is an essential activator of AGC kinases, and most functions of PDK1 are mediated by AGC3 sub-family members, including D6PK/D6PKLs and PAX (Tan et al., 2020;
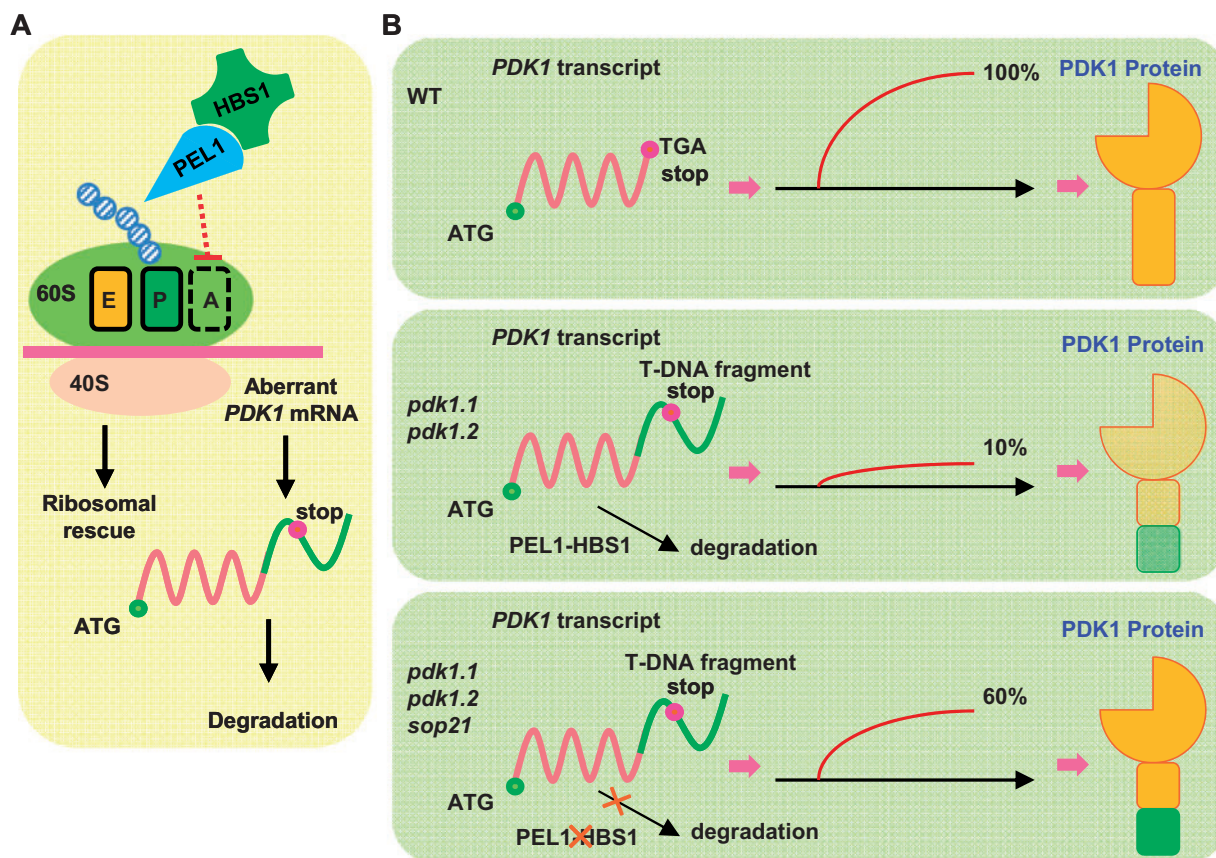
Figure 6 A proposed model showing the function of PEL1–HBS1 mRNA surveillance complex and how *sop21* suppresses *pdk1.1 pdk1.2* phenotypes. A, The PEL1–HBS1 complex regulates 80S ribosomes (composed of a 60S large subunit and a 40S small subunit) through translational surveillance to maintain normal protein translation and plant growth. In the case of truncated *PDK1* transcripts fused with partial T-DNA fragments in *pdk1.1 pdk1.2*, this complex could degrade these aberrant mRNAs, thus promoting the recycling of stalled 80S ribosomes. A-site, ribosomal site most frequently occupied by aminoacyl-tRNA, which functions as an acceptor for the growing protein during peptide bond formation; P-site, ribosomal site most frequently occupied by peptidyl-tRNA, the tRNA carrying the growing peptide chain (blue and white striped circles); E-site, ribosomal site harboring decylated tRNA upon its transit out of the ribosome. B, A proposed model showing *sop21* mutation rescuing the defects of *pdk1.1 pdk1.2*: (1) In WT, the PDK1 transcripts have the stop codon, and can be translated into 100% of PDK1 protein. (2) In the *pdk1.1 pdk1.2* T-DNA mutants, aberrant transcripts with fusion to a partial T-DNA fragment will be recognized by the PEL1–HBS1 complex, and thus get degraded, exhibiting PDK1 loss-of-function mutant defects. (3) The *sop21* mutation leads to the inefficient degradation of aberrant transcripts, which produce enough truncated PDK1 protein to maintain normal growth of *pdk1.1 pdk1.2* plants.

Xiao and Offringa, 2020). Therefore, we checked the protein levels of the known PDK1 substrates from the AGC family in the proteomic datasets. There is an increase of D6PK protein, an essential downstream component of PDK1 (Tan et al., 2020), in *pdk1.1 pdk1.2*, but a relatively lower level of D6PK in *pdk1.1 pdk1.2 pel1* (Supplemental Figure S11A). No dramatic changes were found for other detected AGC proteins in the proteomics data (Supplemental Figure S11, A and B). Therefore, it is very unlikely that changes of these AGC substrates might account for the rescue of *pdk1.1 pdk1.2* by the *pel1* mutation. In line with the notion that PDK1 activates AGC kinases via direct phosphorylation (Tan et al., 2020; Xiao and Offringa, 2020), this type of regulation does not appear to impact AGC protein stability.

Discussion

PDK1 is highly conserved in eukaryotes and is essential for growth and development of various organisms (Pearce et al., 2010). PDK1 deficiency results in severe growth defects or even lethality, which have impeded studies on the molecular mechanism underlying these defects, especially in mammals (Lawlor et al., 2002). By taking advantage of plant genetics and by screening for suppressors that rescue the growth defects of T-DNA insertional *pdk1.1 pdk1.2* mutants, we here identify PEL1, which is a component of the PEL1–HBS1 mRNA surveillance complex and is essential for mRNA quality control during protein translation (Csorba et al., 2018). Our studies reveal that the PEL1–HBS1 complex coordinates ribosome rescue and protein biosynthesis (Figure 6A), and elucidate the mechanism for the *pel1* and *hbs1* mutations that suppress *pdk1.1 pdk1.2* phenotype. That is, the inability of the PEL1–HBS1 complex to degrade aberrant mRNAs leads to the production of truncated but functional PDK1 proteins (Figure 6, A and B).

The PEL1–HBS1 complex plays important roles in the mRNA quality control (Tsuboi et al., 2012; Csorba et al.,

2018). Our study is a typical example of how this mRNA surveillance system regulates the stability of aberrant transcripts. Intriguingly, loss of function of DOM34p or PELOTA causes mitotic arrest in yeast and fruit fly, and the *pelota* mutation is lethal in mouse (Adham et al., 2003), whereas the Arabidopsis mutants *sop21*, *pel1*, and *hbs1* are viable, suggesting a different regulatory mode for regulation of protein translation. Though the *pdk1.1 pdk1.2* double mutant exhibits pleiotropic defects throughout growth and development, the mutant can complete a lifecycle (Tan et al., 2020). It is speculated that the difference might be related to the high post-embryonic developmental plasticity in plants compared with animals, owing to the sessile lifestyle of land plants during evolution.

AGC kinases, D6PK/D6PKLs and PAX, are critical downstream components of PDK1.1 and PDK1.2 in Arabidopsis (Tan et al., 2020; Xiao and Offringa, 2020). Our proteomics analysis indicates that the PEL1–HBS1 complex and PDK1 play pivotal roles in modulating the activity of protein synthesis machinery under normal conditions. Notably, >80% RCE proteins exhibit increased abundances in *pdk1.1 pdk1.2*, and the changed levels are reversed by the *pel1* mutation, suggesting a rescue at the proteome level. Given the lipid binding property of PDK1 and the localizations of PDK1 at the PM, cytoplasm, and certain ER-associated compartments, the pathway proposed here might be responsive to lipid dynamics at the membrane. Further characterization of the exact role of lipids in this process will help to elucidate the molecular mechanistic framework underlying the control of cell growth. In animals, PDK1 can phosphorylate AGC kinases AKT (a.k.a. Protein Kinase B) and S6K, to regulate protein biosynthesis through modulating 40S ribosomal proteins 6S-A (RPS6A) and B (RPS6B), two subunits of ribosomes (Rintelen et al., 2001; Pearce et al., 2010). There are also two S6K homologs, S6K1 and S6K2, in Arabidopsis, previously reported to regulate protein synthesis via RPS6A/B (Mahfouz et al., 2006; Kim et al., 2014). In vitro kinase assays suggest that S6K1 and S6K2 are substrates of Arabidopsis PDK1 (Mahfouz et al., 2006). However, whether these two S6Ks are functionally regulated by PDK1 in planta requires further investigation.*pdk1.1 pdk1.2* exhibits pleotropic growth and developmental defects, and multiple components and pathways might be influenced through AGC kinases by PDK1. For example, *pdk1.1 pdk1.2* shows substantially reduced fertility, which may be due to the changed levels of embryonic development-related proteins EMB1923, RESURRECTION1 (RST1; Chen et al., 2005; Lange et al., 2019; Li et al., 2019; Zhao et al., 2019) and YELLOW STRIPE-LIKE3 (YSL3; Waters et al., 2006). Notably, RST1 is a crucial regulator for RNA metabolism and thus the post-transcriptional gene silencing pathway (Lange et al., 2019; Li et al., 2019). Together with the previous biochemical evidence showing that RST1 forms a complex with HBS1 (SKI7) to act in post-transcriptional gene silencing (Lange et al., 2019), we cannot exclude that PDK1 might be involved in the regulation of PEL1–HBS1-mediated mRNA surveillance mechanisms. Moreover, RST1 was recently identified as a regulator of the vacuolar protein degradation pathway (Zhao et al., 2019), implying a role of PDK1 in the endomembrane trafficking process. Interestingly, precursors of two major storage proteins, 2S albumin and 12S globulin (Shimada et al., 2003; Li et al., 2011; Table 1; Supplemental Tables S3 and S4) are accumulated in *pdk1.1 pdk1.2* shoots at significantly higher levels. Likewise, a number of nutrient reserve-related proteins including lipid transfer protein LTP3 (LIPID-TRANSFER PROTEIN3; Guo et al., 2013), lipoxygenase protein LIPOXYGENASE2 (Tang et al., 2012), oleosin OLEO2 (OLEOSIN2; Choy et al., 2008), and seed-specific protein AT2G05580 (Umezawa et al., 2006) exhibited the same change of protein levels in *pdk1.1 pdk1.2*. Storage proteins are actively synthesized at rough ER as precursor forms and then are transported into protein storage vacuole (PSV) during seed maturation (Li et al., 2006). In angiosperms, seed storage proteins are deposited in PSVs of dry seeds as a source of nitrogen for growth after seed germination (Müntz, 1998; Li et al., 2006). Accumulation of seed storage proteins and nutrient reserve-related proteins in *pdk1.1 pdk1.2* shoots may result in the altered vegetative growth. This indicates that PDK1 represses seed storage proteins and nutrient reserve-related proteins in the vegetative tissues or the nitrogen utilization after seed germination.

It is noteworthy that the *pdk1.1 pdk1.2* phenotype is not fully rescued by *pel1* mutations, or by a truncated *PDK1.1N* transgene. We speculate that the truncated PDK1 protein retains only partial functionality. Meanwhile, PDK1 may also regulate specific life activities through phosphorylating distinct substrates, including those well-characterized AGC kinases as well as possible other players (Zegzouti et al., 2006b; Tan et al., 2020). How these downstream pathways coordinate with each other in space and time needs further investigation.

Materials and methods

Materials and growth conditions

Arabidopsis thaliana lines used in this study were all in ecotype Columbia (Col-0) background. Seeds of Col-0 and various mutants, transgenic lines were germinated on Murashige and Skoog (Duchefa) medium after 2 d' stratification at 4°C. Seedlings and plants were grown in a phytotron at 22°C with a 16-h light/8-h dark photoperiod. Root growth measurements were performed using 14-d-old seedlings grown on Murashige and Skoog medium.

Mutant lines *pdk1.1-2* (*pdk1.1*, SALK_113251C; Tan et al., 2020), *pdk1.2-4* (*pdk1.2*, SALK_017433; Tan et al., 2020), *pdk1.2-2* (*pdk2-4*, SAIL_62_G04; Xiao and Offringa, 2020), *pdk1.2-3* (*pdk2-1*, SAIL_450_B01; Xiao and Offringa, 2020), *pel1* (*pel1*, SALK_124403C), and *hbs1* (*hbs1*, CS857798) were obtained from ABRC (Alonso et al., 2003; Arabidopsis Biological Resource Center) and were genotyped by using corresponding LB, RP, and LP primers (Supplemental Table 7). *pPDK1.1::GUS* and *pPDK1.2::GUS* were reported previously (Tan et al., 2020). *pdk1.1-14 pdk1.2-2* (=*pdk1-14 pdk2-4*),

pdk1.1-13 pdk1.2-3 (=*pdk1-13 pdk2-1*), and *pdk1.1-13 pdk1.2-2* (=*pdk1-13 pdk2-4*) were reported previously (Xiao and Offringa, 2020). The floral dip method (Clough and Bent, 1998) was used for plant transformation.

RT-qPCR analysis

Total RNA was extracted from seedlings using TRIzolR reagent (Life Technologies, 15596-018), incubated with DNAase and reverse transcribed with a TAKARA Primescript ™RT Reagent Kit with gDNA Eraser (RR037A). Transcription of corresponding genes and *ACTIN7* (*AT5G09810*, used as internal reference) was analyzed using SYBR Premix Ex Taq (TAKARA, RR420A) with a BIO-RAD CFX Connect Real-Time System. Relative expression of examined genes was first normalized to *ACTIN7*, and then calculated by setting the gene expression level of WT as "1", and was presented as average ± standard deviation (SD) from three independent biological replicates.

Promoter::β-glucuronidase staining for expression pattern analysis

pPDK1.1::GUS and *pPDK1.2::GUS* transgenic lines were generated previously (Tan et al., 2020), and the *pPEL1::GUS* line (1.5-kb genomic sequence upstream of *PEL1* ATG was used) was generated with a modified pCambia1300 binary vector (Liu et al., 2003) using primers listed in Supplemental Table S7. Stable transgenic lines were stained at 37°C for 1 h, in β-glucuronidase (GUS) solution [0.5-mg·mL^{-1} 5-bromo-4-chloro-3-indolyl-β-d-glucuronic acid (X-Gluc), 0.5-mM potassium ferricyanide (K$_4$[Fe(CN)$_6$]·3H$_2$O), 0.5-mM potassium ferrocyanide (K$_3$[Fe(CN)$_6$]), 0.1% (v/v) Triton X-100, 10-mM ethylenediaminetetraacetic acid (EDTA), and 0.1-M sodium phosphate (NaH$_2$PO$_4$); pH 7.0] (Tan et al., 2020). Three independent lines were analyzed in detail for different tissues and stages, and they all showed similar expression patterns. Samples were imaged by a stereomicroscope (Nikon SMZ1500).

Yeast two-hybrid assay

Yeast two-hybrid (Y2H) assays were performed as reported previously (Tan and Xue, 2014). The coding sequence of *PEL1* was amplified by PCR with PEL1-F (*BamH*I)-3 and PEL1-R (*BamH*I) primers, and was then subcloned into the pGBKT7 vector (Clontech). Coding sequences of HBS1 [using primers HBS1-F (*EcoR*I) and HBS1-R (*BamH*I)] and HBS1 [using primers HBS1-2-F (*Nde*I) and HBS1-2-R (*BamH*I)] were amplified and subcloned into pGADT7 vectors (Clontech). Primers are listed in Supplemental Table S7. Bait and prey plasmids were co-transformed into the yeast strain AH109 according to the manufacture's introduction (Clontech). Transformants were selected on SD (-Leu/-Trp) solid medium. For auxotroph assays, four individual colonies were cultured in liquid SD (-Leu/-Trp) medium overnight, and ~10 μL of each sample at different dilutions (as indicated in the figure legends) was dropped on SD (-Leu/-Trp/-His) medium supplemented with 0.5 mg·mL^{-1} X-α-Gal or on SD (-Leu/-Trp/-His/-Ade) medium, with 1 mM 3-amino-1,2,4-triazole (3-AT), and grown at 30°C for 3 d. Colonies showing continuous growth with a blue color represented interactions.

BiFC assay

For BiFC assay, cDNAs encoding *PDK1.1*, *PDK1.2*, *PEL1*, and *HBS1* were cloned into the pENTR plasmid with BP reactions. Afterward, LR reactions were conducted with the 35S::GW-nYFP and 35S::GW-cYFP destination vectors (Nakamura et al., 2010), resulting in *35S::PDK1.1-nYFP*, *35S::PDK1.1-cYFP*, *35S::PDK1.2-nYFP*, *35S::PDK1.2-cYFP*, *35S::PEL1-nYFP*, and *35S::HBS1-cYFP*. Resultant constructs with control blank vectors were co-expressed in *Nicotiana benthamiana* leaves and yellow fluorescence was observed by a Leica SP8 confocal laser scanning microscope, using an argon laser excitation wavelength of 488 nm after infiltration for 48 h. The emission wavelengths are 520–550 nm.

Subcellular localization and co-localization studies

For subcellular localization studies, cDNAs encoding *PDK1.1*, *PDK1.2*, *PEL1*, and *HBS1* were first cloned into the pENTR plasmid with BP reactions. Afterward, LR reactions were conducted with the pGWB605 destination vector, resulting in *pGWB605-35S::PDK1.1–GFP*, *pGWB605-35S::PDK1.2–GFP*, *pGWB605-35S::PEL1–GFP*, and *pGWB605-35S::HBS1–GFP*, respectively. PDK1.1–GFP, PDK1.2–GFP, PEL1–GFP, HBS1–GFP, and ER–mCherry (Nelson et al., 2007) fusion proteins were transiently expressed in *N. benthamiana* leaves (Lin et al., 2012). For mCherry fusion studies, *PDK1.1* and *PEL1* were cloned into the pB7m24GW2 destination vector. 35S::GFP-HDEL was used for the ER reporter. The infiltrated leaves were harvested 2 d after infiltration and observed using an Olympus confocal microscope (Olympus, FV10i) or a LSM800 confocal laser scanning microscope (Zeiss). PDK1.1–YFP, PDK1.2–YFP, PEL1–YFP, and HBS1–YFP were cloned into the pA7 plasmid and transiently expressed in leaf protoplasts of WT Arabidopsis seedlings expressing ER–mCherry (Nelson et al., 2007), or PIP2-RFP (Yang et al., 2016). Transformed protoplasts were harvested 12 h after transformation and observed using an Olympus confocal microscope (Olympus, FV10i).

For *35S::PDK1.1–GFP*, *35S::PDK1.2–GFP*, and *35S::PEL1–GFP* transgenic plants, entry vectors were reacted with pB7FWG2,0 plasmids for GFP fusion expression. Transformation was performed with the floral dip method (Clough and Bent, 1998) with the *Agrobacterium tumefaciens* strain GV3101. More than 10 T$_1$ lines were selected by Basta resistance and checked by the fluorescence signal. At least three independent lines were analyzed for T$_3$ homozygous lines, and similar subcellular localizations were observed.

Images were captured with following excitation (Ex) and emission (Em) wavelengths (Ex/Em): GFP 488 nm/501–528 nm/YFP 490 nm/520–550 nm; mCherry/RFP 543 nm/620–630 nm; DAPI 405 nm/437–476 nm. Images are analyzed with the Fiji program (SchindeLin et al., 2012).

Protein extraction and Western blot analysis

To examine the protein levels of FLAG- and GFP-tagged proteins, ~100 mg of plant tissues were frozen in liquid nitrogen, ground thoroughly, and homogenized in 100-μL protein extraction buffer [20-mM Tris–HCl, pH 7.5, 150-mM NaCl, 0.5% (v/v) Tween-20, 1-mM EDTA, 1-mM 1,4-dithiothreitol (DTT)] containing a protease inhibitor cocktail (cOmplete, Roche) and a protein phosphatase inhibitor tablet (PhosSTOP, Roche). After addition of sodium dodecyl sulfate loading buffer, the samples were heated at 65°C for 5 min, resolved by 10% (v/v) sodium dodecyl sulfate–polyacrylamide gel electrophoresis (SDS–PAGE) and transferred to polyvinylidene fluoride membranes. FLAG-tagged proteins were detected by a mouse anti-FLAG antibody (M20008, 1:2,000, Abmart). GFP-tagged proteins were detected with a mouse anti-GFP antibody (M20004, 1:2,000, Abmart) or a mouse anti-GFP HRP (horseradish peroxidase)-conjugated antibody (130-091-833, 1:2,000, MACS Molecular). Actin was detected by a mouse anti-actin antibody (M20009, 1:2,000, Abmart).

After incubation with a primary mouse antibody, the PVDF membrane was then incubated with a goat anti-mouse immunoglobulin G AP-conjugated secondary antibody (ab97020, 1:5,000, Abcam). AP activity was detected by BCIP/NBT kit (Invitrogen) according to the supplier's instructions. HRP activity was detected by the Supersignal Western Detection Reagents (Thermo Scientific).

Protein expression and purification

Coding regions of PDK1.1, PEL1, and HBS1 were amplified with corresponding primers, and subcloned into vectors pET28a (Novagen) or pGEX-4T-1 (GE Healthcare). Proteins were recombinantly expressed in *Escherichia coli* (strain BL21) by supplementing with 1-mM or 0.2-mM isopropyl-β-ᴅ-thiogalactopyranoside (induced at either 28°C for 3 h or 16°C for 16 h). Fusion proteins with His tag were purified using Ni-NTA His binding resin (Novagen) and those with GST tag were purified by glutathione sepharose (Novagen).

GST pull-down assay

GST pull-down assay for testing the interaction between GST–HBS1 and His–PEL1 was performed as reported previously (Tan and Xue, 2014; Tan et al., 2020). GST–HBS1 and His–PEL1 proteins were expressed and purified in *E. coli* (strain BL21). A 1 mL of GST (as control; this assay used relatively less volume due to a higher protein yield than GST–HBS1) and 15-mL GST–HBS1 lysates were incubated with 100-μL GST binding resin for 30 min in 1.5 mL tubes at 4°C. Samples were spun down at 3,000 *g* for 1 min, and the supernatant was discarded. The pellet was washed with 400-μL 1×TBS (50-mM Tris–HCl, 150-mM NaCl, pH 7.6). Around 200-μL purified His–PEL1 (about 0.5 μg·μL^{-1}) was added into each tube, plus another 400-μL 1×TBS, and then incubated at 4°C for 30 min. Afterward, the samples were spun down at 3,000 *g* for 1 min, and then washed with 500 μL 1×TBS for three times. The resin was finally re-suspended in 30-μL elution buffer (1×TBS, 10-mM glutathione), and the sample was then added with 15-μL SDS loading dye. Twenty microliter samples were separated with 12% (v/v) SDS–PAGE, and detected by Western blot. His-tagged proteins were detected by a mouse anti-His antibody (sc-8036, 1:3,000, Santa Cruz Biotechnology). GST-tagged proteins were detected by a mouse anti-GST antibody (sc-138, 1:3,000, Santa Cruz Biotechnology).

A TMT-based comparative proteomics analysis

A TMT-based comparative proteomics analysis was performed according to Thompson's research (Thompson et al., 2003). WT (Col-0), *pdk1.1 pdk1.2*, *pdk1.1 pdk1.2 pel1* seedlings were grown on 1/2 Murashige and Skoog dishes for 14 d. One gram of shoots (aerial parts) and 0.6 g roots (underground parts) of three genotypes of seedlings were set as groups 1 and 2, respectively. There are three biological replicates for each genotype.

Samples were frozen in liquid nitrogen and ground homogeneously into powder. TCA/acetone (1:9) at 5× sample volume was added to the powder and mixed by vortexing. The mixture was placed at −20°C for 4 h, and centrifuged at 6,000*g* for 40 min at 4°C. The supernatant was discarded. The pre-cooled acetone was added to wash three times. The pellet was air dried. SDT buffer at 30× (30 μL for 1 mg pellet) sample volume was added to 20–30 mg powder, mixed and boiled for 5 min. The lysate was sonicated and then boiled for 15 min. After centrifuged at 14,000*g* for 40 min, the supernatant was filtered with 0.22-μm filters. The filtrate was quantified with the BCA Protein Assay Kit (Bio-Rad, USA). The sample was stored at −80°C.

Twenty microgram of proteins for each sample were mixed with 5× loading buffer respectively and boiled for 5 min. Proteins were separated with 12.5% (v/v) SDS–PAGE (constant current 14 mA, 90 min) and bands were visualized by Coomassie Blue R-250 staining.

Two hundred microgram of proteins for each sample were incorporated into 30-μL SDT buffer [4% SDS (w/v), 100-mM DTT, 150-mM Tris–HCl, pH 8.0]. The detergent, DTT, and other low-molecular-weight components were removed using UA buffer (8-M Urea, 150-mM Tris–HCl, pH 8.0) by repeated ultrafiltration (Microcon units, 10 kDa). Then 100-μL iodoacetamide (100-mM iodoacetamide in UA buffer) was added to block reduced cysteine residues, and the samples were incubated for 30 min in darkness. The filters were washed with 100-μL UA buffer three times and then with 100-μL 100-mM triethylammonium bicarbonate (TEAB) buffer twice. Finally, the protein suspensions were digested with 4-μg trypsin (Promega) in 40-μL TEAB buffer overnight at 37°C, and the resulting peptides were collected as a filtrate. The peptide content was estimated by UV light spectral density at 280 nm using an extinction coefficient of 1.1 of 0.1% (w/v) solution that was calculated on the basis of the frequency of tryptophan and tyrosine in vertebrate proteins.

One hundred micrograms peptide mixture of each sample was labeled using TMT reagent according to the manufacturer's instructions (Thermo Fisher Scientific) and analyzed

on an Orbitrap Fusion Lumos (Thermo Scientific) mass spectrometer coupled with Ultimate 3000 RSLC nano system. Four microliters of each fraction was injected for nano liquid chromatography–tandem mass spectrometry (LC–MS/MS) analysis. The peptide mixture (1 μg) was loaded onto the Acclaim PepMap 100 analytical column (75 μm × 15 cm, C18, 3 μm, Thermo Scientific) in buffer A [0.1% (v/v) Formic acid] and separated with a linear gradient of buffer B [80% (v/v) acetonitrile and 0.1% (v/v) Formic acid] at a flow rate of 300 nL·min^{-1}. The electrospray voltage of 2.1 kV, versus the inlet of the mass spectrometer, was used. Mass spectrometer was operated in the data-dependent mode to switch automatically between mass spectrometry (MS) and tandem mass spectrometry (MS/MS) acquisition with a cycle time of 3 s. Survey full-scan MS spectra (m/z 375–1,800) were acquired with a mass resolution of 120 K, followed by sequential high energy collisional dissociation MS/MS scans with a resolution of 50K. In all cases, one microscan was recorded using dynamic exclusion of 40 s. For MS/MS, precursor ions were activated using 38% normalized collision energy.

MS/MS spectra were analyzed using ProteinDiscoverer Software 2.1 against the TAIR10_pep_20101214 database and decoy database with following parameters. The highest score for a given peptide mass (best match to that predicted in the database) was used to identify parent proteins. Parameters for protein searching were set as follows: tryptic digestion with at most two missed cleavages, carbamidomethylation of cysteines as fixed modification, and oxidation of methionines and protein N-terminal acetylation as variable modifications. Peptide spectral matches were validated based on q-values at a 1% false discovery rate.

Proteins were considered differentially expressed when they displayed significant changes between two groups of datasets (>1.2-fold by analysis of variance (ANOVA), $p <$ 0.05). Adjusted p-values were calculated using the Tukey's honestly significant difference method. Relative levels of the analyzed proteins (the values of abundance divided by 100) were used to perform the hierarchical clustering analysis using the OECloud tools at https://cloud.oebiotech.cn

The FASTA protein sequences of differentially changed proteins were blasted against the online Kyoto Encyclopedia of Genes and Genomes (KEGG) database (http://geneontology.org/) to retrieve their KOs and were subsequently mapped to pathways in KEGG. The corresponding KEGG pathways were extracted.

Quantification and statistics

Lateral root numbers were counted directly. For measurements of silique length, primary root length, and leaf area, photos were analyzed with the Image J program (https://imagej.nih.gov/ij/download.html). Fluorescence intensities of reporter lines were analyzed and quantified by Fiji (https://fiji.sc/; SchindeLin et al., 2012). Data visualization and statistics were performed with GraphPad Prism8. Student's t test was used for comparing two data sets, and one-way ANOVA with a Tukey's test was performed for multiple

comparisons. Statistical analysis for the TMT-proteomics data was performed using the OECloud tools at https://cloud.oebiotech.cn.

Accession numbers

Sequence data from this article can be found in the GenBank/EMBL data libraries under the following accession numbers: PDK1.1 (AT5G04510), PDK1.2 (AT3G10540), PEL1 (AT4G27650), HBS1 (AT5G10630), D6PK (AT5G55910), D6PKL1 (AT4G26610), D6PKL2 (AT5G47750), D6PKL3 (AT3G27580), PID (AT2G34650), OXI1/AGC2-1 (AT3G25250), GAT 1_2.1 (AT1G15040), SRPP (AT4G02270), PRPL1 (AT5G05500), DGR1 (AT1G80240), DGR2 (AT5G25460), GH9C1 (AT1G48930), DER9 (AT5G49270), LTP3 (AT5G59320), LOX2 (AT3G45140), and OLEO2 (AT5G40420).

Supplemental data

The following materials are available in the online version of this article.

Supplemental Figure S1. Expression profiles of *PDK1.1* and *PDK1.2*.

Supplemental Figure S2. Identification of the *pel1* mutant.

Supplemental Figure S3. Expression profiles of *PEL1*.

Supplemental Figure S4. Loss of function of *PEL1* suppresses the defective growth of *pdk1.1 pdk1.2*, confirmed by complementation.

Supplemental Figure S5. Sequence alignment among *Arabidopsis thaliana* HBS1, *Homo sapiens* HBS1, and *Saccharomyces cerevisiae* HBS1.

Supplemental Figure S6. Identification of *hbs1* mutants.

Supplemental Figure S7. Phenotypes of multiple combinations of *pdk1.1 pdk1.2* double mutants.

Supplemental Figure S8. Increased expression of PDK1 N-terminal fragments rescued the growth defects of *pdk1.1 pdk1.2*.

Supplemental Figure S9. Subcellular localization of PDK1.1-YFP, PDK1.2-YFP, PEL1-YFP, and HBS1-YFP.

Supplemental Figure S10. PDK1 doesn't affect the amounts of PEL1 and HBS1 proteins.

Supplemental Figure S11. Abundance of AGC protein kinases in *pdk1.1 pdk1.2* or *pdk1.1 pdk1.2 pel1*.

Supplemental Table S1. Proteins identified by analyzing shoot proteomes of Col-0, *pdk1.1 pdk1.2*, *pdk1.1 pdk1.2 pel1* mutants by TMT-based proteomics.

Supplemental Table S2. Proteins identified by analyzing root proteomes of Col-0, *pdk1.1 pdk1.2*, and *pdk1.1 pdk1.2 pel1* mutants by TMT-based proteomics.

Supplemental Table S3. RCEs identified in shoots by analyzing Col-0, *pdk1.1 pdk1.2*, and *pdk1.1 pdk1.2 pel1* mutants.

Supplemental Table S4. Differentially expressed proteins in shoots identified by analyzing Col-0 and *pdk1.1 pdk1.2* mutants.

Supplemental Table S5. restored CE proteins identified in roots by analyzing Col-0, *pdk1.1 pdk1.2*, and *pdk1.1 pdk1.2 pel1* mutants.

Supplemental Table S6. Differentially expressed proteins in roots identified by analyzing Col-0 and *pdk1.1 pdk1.2* mutants.

Supplemental Table S7. Primers used in this study.

Data and materials availability

All data and materials necessary to evaluate the conclusions in the article or supplementary materials are available.

References

Adham IM, Sallam MA, Steding G, Korabiowska M, Brinck U, Hoyer-fender S, Oh C, Engel W (2003) Disruption of the *Pelota* gene causes early embryonic lethality and defects in cell cycle progression. Mol Cell Biol **23:** 1470–1476

Alessi DR (2001) Discovery of PDK1, one of the missing links in insulin signal transduction. Biochem Soc Trans **29:** 1–14

Allen RS, Nakasugi K, Doran RL, Millar AA, Waterhouse PM (2013) Facile mutant identification via a single parental backcross method and application of whole genome sequencing based mapping pipelines. Front Plant Sci **4:** 362

Alonso JM, Curran T, Hawkes R, Soriano P, Cooper JA, Lichtman JW, Bernier B, Goffinet AM, Derer M, Goffinet A, et al. (2003) Genome-wide insertional mutagenesis of *Arabidopsis thaliana*. Science **301:** 653–657

Anthony RG, Henriques R, Helfer A, Mészáros T, Rios G, Testerink C, Munnik T, Deák M, Koncz C, Bögre L (2004) A protein kinase target of a PDK1 signalling pathway is involved in root hair growth in *Arabidopsis*. EMBO J **23:** 572–581

Boron AK, Orden J Van, Markakis MN, Mouille G, Adriaensen D, Verbelen JP, Höfte H, Vissenberg K (2014) Proline-rich protein-like PRPL1 controls elongation of root hairs in *Arabidopsis thaliana*. J Exp Bot **65:** 5485–5495

Breitenbach HH, Wenig M, Wittek F, Jorda L, Maldonado-Alconada AM, Sarioglu H, Colby T, Knappe C, Bichlmeier M, Pabst E, et al. (2014) Contrasting roles of apoplastic aspartyl protease AED1 and legume lectin-like protein LLP1 in *Arabidopsis* systemic acquired resistance. Plant Physiol **165:** 791–809

Brunkard JO, Baker B (2018) A two-headed monster to avert disaster: HBS1/SKI7 is alternatively spliced to build eukaryotic RNA surveillance complexes. Front Plant Sci **9:** 1333

Camehl I, Drzewiecki C, Vadassery J, Shahollari B, Sherameti I, Forzani C, Munnik T, Hirt H, Oelmüller R (2011) The OXI1 kinase pathway mediates *Piriformospora indica*-induced growth promotion in *Arabidopsis*. PLoS Pathog **7:** e1002051

Del Campillo E, Gaddam S, Mettle-Amuah D, Heneks J (2012) A tale of two tissues: AtGH9C1 is an endo-β-1,4-glucanase involved in root hair and endosperm development in *Arabidopsis*. PLoS One **7:** e49363

Casamayor A, Torrance PD, Kobayashi T, Thorner J, Alessi DR (1999) Functional counterparts of mammalian protein kinases PDK1 and SGK in budding yeast. Curr Biol **9:** 186–197

Chen CC, Chien WF, Lin NC, Yeh KC (2014) Alternative functions of Arabidopsis YELLOW STRIPELIKE3: from metal translocation to pathogen defense. PLoS One **9:** e98008

Chen X, Goodwin SM, Liu X, Chen X, Bressan RA, Jenks MA (2005) Mutation of the *RESURRECTION1* locus of *Arabidopsis* reveals an association of cuticular wax with embryo development. Plant Physiol **139:** 909–919

Choy MK, Sullivan JA, Theobald JC, Davies WJ, Gray JC (2008) An *Arabidopsis* mutant able to green after extended dark periods shows decreased transcripts of seed protein genes and altered sensitivity to abscisic acid. J Exp Bot **59:** 3869–3884

Clough SJ, Bent AF (1998) Floral dip: a simplified method for *Agrobacterium*-mediated transformation of *Arabidopsis thaliana*. Plant J **16:** 735–743

Csorba T, Auber A, Schamberger A (2018) The nonstop decay and the RNA silencing systems operate cooperatively in plants. Nucleic Acids Res **46:** 4632–4648

Deak M, Casamayor A, Currie RA, Peter Downes C, Alessi DR (1999) Characterisation of a plant 3-phosphoinositide-dependent protein kinase-1 homologue which contains a pleckstrin homology domain. FEBS Lett **451:** 220–226

Dittrich ACN, Devarenne TP (2012) Characterization of a PDK1 homologue from the moss *Physcomitrella patens*. Plant Physiol **158:** 1018–1033

Dyson BC, Miller MAE, Feil R, Rattray N, Bowsher CG, Goodacre R, Lunn JE, Johnson GN (2016) FUM2, a cytosolic fumarase, is essential for acclimation to low temperature in *Arabidopsis thaliana*. Plant Physiol **172:** 118–127

Ferrari S (2003) Tandemly duplicated *Arabidopsis* genes that encode polygalacturonase-inhibiting proteins are regulated coordinately by different signal transduction pathways in response to fungal infection. Plant Cell **15:** 93–106

Ferrari S, Galletti R, Vairo D, Cervone F, De Lorenzo G (2007) Antisense expression of the *Arabidopsis thaliana* AtPGIP1 gene reduces polygalacturonase-inhibiting protein accumulation and enhances susceptibility to *Botrytis cinerea*. Mol Plant-Microbe Interact **19:** 931–936

Friml J, Yang X, Michniewicz M, Weijers D, Quint A, Tietz O, Benjamins R, Ouwerkerk PBF, Ljung K, Sandberg G, et al. (2004) A PINOID-dependent binary switch in apical-basal PIN polar targeting directs auxin efflux. Science **306:** 862–865

Gao Y, Badejo AA, Sawa Y, Ishikawa T (2012) Analysis of two L-Galactono-1,4-Lactone-responsive genes with complementary expression during the development of *Arabidopsis thaliana*. Plant Cell Physiol **53:** 592–601

Guo L, Yang H, Zhang X, Yang S (2013) *Lipid transfer protein 3* as a target of MYB96 mediates freezing and drought stress in *Arabidopsis*. J Exp Bot **64:** 1755–1767

Hilal T, Yamamoto H, Loerke J, Mielke T, Spahn CMT (2016) Structural insights into ribosomal rescue by Dom34 and Hbs1 at near-atomic resolution. Nat Commun **7:** 13521

Horvath DP, Mclarney BK, Thomashow MF (1993) Regulation of *Arabidopsis thaliana* L. (Heyn) *cor78* in response to low temperature. Plant Physiol **103**: 1047–1053

Inagaki M, Schmelzle T, Yamaguchi K, Irie K, Hall MN, Matsumoto K (1999) PDK1 homologs activate the Pkc1-mitogen-activated protein kinase pathway in yeast. Mol Cell Biol **19**: 8344–8352

Jung J, Kumar K, Lee HY, Park Y-I, Cho H-T, Ryu SB (2012) Translocation of phospholipase A2α to apoplasts is modulated by developmental stages and bacterial infection in *Arabidopsis*. Front Plant Sci **3**: 126

Kim Y-K, Kim S, Shin Y, Hur Y-S, Kim W-Y, Lee M-S, Cheon C-I, Verma DPS (2014) Ribosomal protein S6, a target of rapamycin, is involved in the regulation of of rRNA genes by possible epigenetic changes in *Arabidopsis*. J Biol Chem **289**: 3901–3912

Lange H, Ndecky SYA, Gomez-diaz C, David P, Butel N, Zumsteg J, Kuhn L, Piermaria C, Chicher J, Christie M, et al. (2019) RST1 and RIPR connect the cytosolic RNA exosome to the Ski complex in *Arabidopsis*. Nat Commun **10**: 3871

Lawlor MA, Mora A, Ashby PR, Williams MR, Murray-Tait V, Malone L, Prescott AR, Lucocq JM, Alessi DR (2002) Essential role of PDK1 in regulating cell size and development in mice. EMBO J **21**: 3728–3738

Li L, Shimada T, Takahashi H, Ueda H, Fukao Y, Kondo M, Nishimura M, Hara-Nishimura I (2006) MAIGO2 is involved in exit of seed storage proteins from the endoplasmic reticulum in *Arabidopsis thaliana*. Plant Cell **18**: 3535–3547

Li Q, Wang B-C, Xu Y, Zhu Y-X (2011) Systematic studies of 12S seed storage protein accumulation and degradation patterns during *Arabidopsis* seed maturation and early seedling germination stages. J Biochem Mol Biol **40**: 373–381

Li T, Natran A, Chen Y, Vercruysse J, Wang K, Gonzalez N, Dubois M, Inzé D (2019) A genetics screen highlights emerging roles for CPL3, RST1 and URT1 in RNA metabolism and silencing. Nat Plants **5**: 539–550

Lin D, Nagawa S, Chen J, Cao L, Chen X, Xu T, Li H, Dhonukshe P, Yamamuro C, Friml J, et al. (2012) A ROP GTPase-dependent auxin signaling pathway regulates the subcellular distribution of PIN2 in *Arabidopsis* roots. Curr Biol **22**: 1319–1325

Liu W, Xu ZH, Luo D, Xue HW (2003) Roles of OsCKI1, a rice casein kinase I, in root development and plant hormone sensitivity. Plant J **36**: 189–202

Mahfouz MM, Kim S, Delauney AJ, Verma DPS (2006) *Arabidopsis* TARGET OF RAPAMYCIN interacts with RAPTOR, which regulates the activity of S6 Kinase in response to osmotic stress signals. Plant Cell **18**: 477–490

Marhava P, Bassukas AEL, Zourelidou M, Kolb M, Moret B, Fastner A, Schulze WX, Cattaneo P, Hammes UZ, Schwechheimer C, et al. (2018) A molecular rheostat adjusts auxin flux to promote root protophloem differentiation. Nature **558**: 297–300

Matsui H, Miyao A, Takahashi A, Hirochika H (2010) Pdk1 kinase regulates basal disease resistance through the OsOxi1-OsPti1a phosphorylation cascade in rice. Plant Cell Physiol **51**: 2082–2091

Mora A, Komander D, Van Aalten DMF, Alessi DR (2004) PDK1, the master regulator of AGC kinase signal transduction. Semin Cell Dev Biol **15**: 161–170

Müntz K (1998) Deposition of storage proteins. Plant Mol Biol **38**: 77–99

Nakamura S, Mano S, Tanaka Y, Ohnishi M, Nakamori C, Araki M, Niwa T, Nishimura M, Kaminaka H, Nakagawa T, et al. (2010) Gateway binary vectors with the bialaphos resistance gene, bar, as a selection marker for plant transformation. Biosci Biotechnol Biochem **74**: 1315–1319

Nelson BK, Cai X, Nebenführ A (2007) A multicolored set of *in vivo* organelle markers for co-localization studies in *Arabidopsis* and other plants. Plant J **51**: 1126–1136

Page DR, Grossniklaus U (2002) The art and design of genetic screens: *Arabidopsis thaliana*. Nat Rev Genet **3**: 124–136

Pearce LR, Komander D, Alessi DR (2010) The nuts and bolts of AGC protein kinases. Nat Rev Mol Cell Biol **11**: 9–22

Pisareva VP, Skabkin MA, Hellen CUT, Pestova T V., Pisarev A V. (2011) Dissociation by Pelota, Hbs1 and ABCE1 of mammalian vacant 80S ribosomes and stalled elongation complexes. EMBO J **30**: 1804–1817

Qin P, Fan S, Deng L, Zhong G, Zhang S, Li M, Chen W, Wang G, Tu B, Wang Y, et al. (2018) *LML1*, encoding a conserved eukaryotic Release Factor 1 protein, regulates cell death and pathogen resistance by forming a conserved complex with SPL33 in rice. Plant Cell Physiol **59**: 887–902

Rentel MC, Lecourieux D, Ouaked F, Usher SL, Petersen L, Okamoto H, Knight H, Peck SC, Grierson CS, Hirt H, et al. (2004) OXI1 kinase is necessary for oxidative burst-mediated signalling in *Arabidopsis*. Nature **427**: 858–861

Ringli C, Baumberger N, Keller B (2005) The *Arabidopsis* root hair mutants *der2-der9* are affected at different stages of root hair development. Plant Cell Physiol **46**: 1046–1053

Rintelen F, Stocker H, Thomas G, Hafen E (2001) PDK1 regulates growth through Akt and S6K in *Drosophila*. Proc Natl Acad Sci U S A **98**: 15020–15025

Saito S, Hosoda N, Hoshino SI (2013) The Hbs1-Dom34 protein complex functions in non-stop mRNA decay in mammalian cells. J Biol Chem **288**: 17832–17843

Schindelin J, Arganda-Carreras I, Frise E, Kaynig V, Longair M, Pietzsch T, Preibisch S, Rueden C, Saalfeld S, Schmid B, et al. (2012) Fiji: an open-source platform for biological-image analysis. Nat Methods **9**: 676–682

Scholz S, Pleßmann J, Enugutti B, Hüttl R, Wassmer K, Schneitz K (2019) The AGC protein kinase UNICORN controls planar growth by attenuating PDK1 in Arabidopsis thaliana. PLoS Genet **15**: e1007927

Shimada T, Yamada K, Kataoka M, Nakaune S, Koumoto Y, Kuroyanagi M, Tabata S, Kato T, Shinozaki K, Seki M, et al. (2003) Vacuolar processing enzymes are essential for proper processing of seed storage proteins in *Arabidopsis thaliana*. J Biol Chem **278**: 32292–32299

Shoemaker CJ, Eyler DE, Green R (2010) Dom34:Hbs1 promotes subunit dissociation and peptidyl-tRNA drop-off to initiate no-go decay. Science **330**: 369–372

Storz, P., Toker A (2002) 3 -phosphoinositide-dependent kinase-1 PDK-1 in PI 3-kinase signaling. Front Biosci **7**: 886–902

Stotz HU, Sawada Y, Shimada Y, Hirai MY, Sasaki E, Krischke M, Brown PD, Saito K, Kamiya Y (2011) Role of camalexin, indole glucosinolates, and side chain modification of glucosinolate-derived isothiocyanates in defense of *Arabidopsis* against Sclerotinia sclerotiorum. Plant J **67**: 81–93

Tan S-T, Xue H-W (2014) Casein Kinase 1 regulates ethylene synthesis by phosphorylating and promoting the turnover of ACS5. Cell Rep **9**: 1692–1702

Tan S, Luschnig C, Friml J (2021) Pho-view of auxin: reversible protein phosphorylation in auxin biosynthesis, transport and signalling. Mol Plant **14**: 151–165

Tan S, Zhang X, Kong W, Yang X-L, Molnár G, Vondráková Z, Filepová4 R, Petrášek J, Friml J, Xue H-W (2020) The lipid code-dependent phosphoswitch PDK1–D6PK activates PIN-mediated auxin efflux in *Arabidopsis*. Nat Plants **6**: 556–569

Tanaka N, Uno H, Okuda S, Gunji S, Ferjani A, Aoyama T, Maeshima M (2017) SRPP, a cell wall protein is involved in development and protection of seeds and root hairs in *Arabidopsis thaliana*. Plant Cell Physiol **58**: 760–769

Tang X, Lim MH, Pelletier J, Tang M, Nguyen V, Keller WA, Tsang EWT, Wang A, Rothstein SJ, Harada JJ, et al. (2012) Synergistic repression of the embryonic programme by SET DOMAIN GROUP 8 and EMBRYONIC FLOWER 2 in *Arabidopsis* seedlings. J Exp Bot **63**: 1391–1404

Thomma BPHJ, Eggermont K, Mauch-Mani B, Vogelsang R, Cammue BPA, Broekaert WF (1998) Separate jasmonate-dependent and salicylate-dependent defense-response pathways in *Arabidopsis* are essential for resistance to distinct microbial pathogens. Proc Natl Acad Sci U S A **95:** 15107–15111

Thompson A, Schäfer J, Kuhn K, Kienle S, Schwarz J, Schmidt G, Neumann T, Johnstone R, Mohammed AKA, Hamon C (2003) Tandem mass tags: a novel quantification strategy for comparative analysis of complex protein mixtures by MS/MS. Anal Chem **75:** 1895–1904

Tronchet M, BalaguÉ C, Kroj T, Jouanin L, Roby D (2010) Cinnamyl alcohol dehydrogenases-C and D, key enzymes in lignin biosynthesis, play an essential role in disease resistance in *Arabidopsis*. Mol Plant Pathol **11:** 83–92

Tsuboi T, Kuroha K, Kudo K, Makino S, Inoue E, Kashima I, Inada T (2012) Dom34:hbs1 plays a general role in quality-control systems by dissociation of a stalled ribosome at the 3' end of aberrant mRNA. Mol Cell **46:** 518–529

Uemura M, Gilmour SJ, Thomashow MF, Steponkus PL (2002) Effects of COR6.6 and CORl5am polypeptides encoded by *COR (Cold-Regulated)* genes of *Arabidopsis thaliana* on the freeze-induced fusion and leakage of liposomes. Plant Physiol **111:** 313–327

Umezawa T, Fujita Y, Furihata T, Maruyama K, Yamaguchi-Shinozaki K, Shinozaki K, Yoshida R (2006) Abscisic acid-dependent multisite phosphorylation regulates the activity of a transcription activator AREB1. Proc Natl Acad Sci U S A **103:** 1988–1993

Waters BM, Chu H-H, DiDonato RJ, Roberts LA, Eisley RB, Lahner B, Salt DE, Walker EL (2006) Mutations in *Arabidopsis Yellow Stripe-Like1* and *Yellow Stripe-Like3* reveal their roles in metal ion homeostasis and loading of metal ions in seeds. Plant Physiol **141:** 1446–1458

Weis C, Hildebrandt U, Hoffmann T, Hemetsberger C, Pfeilmeier S, König C, Schwab W, Eichmann R, Hückelhoven R (2014) CYP83A1 is required for metabolic compatibility of *Arabidopsis* with the adapted powdery mildew fungus *Erysiphe cruciferarum*. New Phytol **202:** 1310–1319

Xiao Y, Offringa R (2020) PDK1 regulates auxin transport and Arabidopsis vascular development through AGC1 kinase PAX. Nat Plants **6:** 544–555

Yang BJ, Han XX, Yin LL, Xing MQ, Xu ZH, Xue HW (2016) *Arabidopsis PROTEASOME REGULATOR1* is required for auxin-mediated suppression of proteasome activity and regulates auxin signalling. Nat Commun **7:** 11388

Zegzouti H, Anthony RG, Jahchan N, Bogre L, Christensen SK (2006a) Phosphorylation and activation of PINOID by the phospholipid signaling kinase 3-phosphoinositide-dependent protein kinase 1 (PDK1) in *Arabidopsis*. Proc Natl Acad Sci U S A **103:** 6404–6409

Zegzouti H, Li W, Lorenz TC, Xie M, Payne CT, Smith K, Glenny S, Payne GS, Christensen SK (2006b) Structural and functional insights into the regulation of *Arabidopsis* AGC VIIIa kinases. J Biol Chem **281:** 35520–35530

Zhang Y, He J, McCormick S (2009) Two *Arabidopsis* AGC kinases are critical for the polarized growth of pollen tubes. Plant J **58:** 474–484

Zhao Q, Shen J, Gao C, Cui Y, Wang Y, Cui J, Cheng L, Cao W (2019) RST1 is a FREE1 suppressor that negatively regulates vacuolar trafficking in *Arabidopsis*. Plant Cell **31:** 2152–2168

Zhu H, Kranz RG (2012) A nitrogen-regulated glutamine amidotransferase (GAT1_2.1) represses shoot branching in *Arabidopsis*. Plant Physiol **160:** 1770–1780

Zourelidou M, Muller I, Willige BC, Nill C, Jikumaru Y, Li H, Schwechheimer C (2009) The polarly localized D6 PROTEIN KINASE is required for efficient auxin transport in *Arabidopsis thaliana*. Development **136:** 627–636